Excitation functions for the reactions $^{208}Pb(p,n)^{208}Bi$ and $^{208}Pb(p,2n)^{207}Bi$ measured with the AFRODITE γ-ray Spectrometer

Frank Solomon Komati

A thesis submitted in partial fulfillment of the requirements
for the degree of Masters in Applied Radiation Science and Technology
in the Center for Applied Radiation Science and Technology
University of North West

March 2004

Excitation functions for the reactions $^{208}Pb(p,n)^{208}Bi$ and $^{208}Pb(p,2n)^{207}Bi$ measured with the AFRODITE γ-ray Spectrometer

Frank Komati
iThemba LABS, P.O. Box 722, Somerset West, 7129, South Africa
e-mail: fskomati@tlabs.ac.za

Abstract

Excitation functions for the population of ^{207}Bi and ^{208}Bi via the bombardment of a thin ^{208}Pb ($1mg/cm^2$) target with a proton beam having energies of 11.6, 11.9, 13.2 and 14.8 MeV were measured. The corresponding nuclear reactions are $^{208}Pb(p,n)^{208}Bi$ and $^{208}Pb(p,2n)^{207}Bi$. The γ-γ coincidence data associated with the above reactions were measured with the AFRODITE array consisting of 8 Clover detectors. The experiment was conducted at iThemba Laboratory for Accelerator Based Sciences (iThemba LABS).

The analysis involved: the identification of γ-ray transitions associated with the de-excitation of the residual ^{208}Bi and ^{207}Bi nuclei, γ-γ coincidence relationships and the γ intensity measurements. Furthermore, the relationship between the proton incident energy and the intensity of the γ-rays for ^{207}Bi and ^{208}Bi was established. The results show that the $^{208}Pb(p,n)^{208}Bi$ reaction is dominant at E_p = 11.9 MeV, and decreases as the proton energy is increased. The yield from the $^{208}Pb(p,2n)^{207}Bi$ reaction increases monotonically as the proton energy is increased to 14.8 MeV. The data suggest that the maximum yield for this reaction has not reached, and measurements at higher proton energies would be needed to complete the excitation function.

Acknowledgements

The author would like to thank the Almighty, my ancestors and all the people who assisted in making possible the realization of this thesis. Those include my supervisor, Dr. Simon Mullins*, Dr. Matej Lipoglavšek†, iThemba LABS Nuclear Physics Group staff and postgraduate students, The NRF- for their financial support, my family and friends. God Bless!

Frank Solomon Komati, *March 2004*

* iThemba LABS, 7129 Somerset West, South Africa
† Present address: J. Stefan Institute, 1000 Ljubljana, Slovenia

Contents

Chapter 1 Introduction **1**

1.1 Overview ... 1
1.2 Compound Nuclear Reactions Overview ... 1
1.3 Previous Studies ... 6
1.4 Aim of this Study ... 11

Chapter 2 Experimental Techniques and Equipment

2.1 Interaction of γ-rays with matter ... **12**
2.1.1 Photoelectric Effect ... 12
2.1.2 Compton Scattering ... 12
2.1.3 Pair Production ... 14
2.2 Experimental Equipment ... 15
2.2.1 The Facilities at iThemba LABS ... 16
2.2.2 Separated-Sector Cyclotron ... 16
2.2.3 AFRODITE Array ... 16
2.2.4 Clover Detectors ... 18
2.2.5 Compton Suppression ... 20
2.2.6 Proton Beam ... 21
2.2.7 Target ... 24
2.2.8 Electronics and Data Acquisition Systems ... 24
25

Chapter 3 Data Reduction and Analysis Procedure

3.1 The Experiment ... **28**
3.2 Data Analysis ... 28
3.3 Energy and Efficiency Calibration ... 29
3.4 Gain Matching ... 34
3.5 Doppler Shift Corrections ... 36
3.6 E_γ-E_γ matrices ... 36
3.7 Transition Intensities ... 37
38

Chapter 4 Results of Data Analysis **39**

4.1 ^{208}Bi γ-γ coincidences ... 39
4.2 Transition Intensities for ^{208}Bi ... 51
4.3 ^{207}Bi γ-γ coincidences ... 54
4.4 Transition Intensities for ^{207}Bi ... 59
4.5 Discussion ... 63

Chapter 5 Summary and conclusion **66**

Appendix 1A
Determination of the absolute γ-ray transition intensities(I) for the ^{208}Bi residual nuclei from the un-gated spectra at four proton energies. 68

Appendix 1B
Determination of the relative γ-ray transition intensities ($\%I_\gamma$) for the ^{208}Bi residual nuclei normalized to the 601.8 keV transition. 71

Appendix 2A
Determination of the absolute γ-ray transition intensities (I) for the ^{207}Bi residual nuclei from the un-gated spectra at four proton energies. 74

Appendix 2B
Determination of the relative γ-ray transition intensities ($\%I_\gamma$) for the ^{207}Bi residual nuclei normalized to the 742.6 keV transition. 76

References 78

List of Figures

1.1 Bound states in a square well [She03]..... 2
1.2 Stages in the compound nucleus formation process [Mab03]..... 3
1.3 Energy spectra of protons and neutrons emitted from proton induced reactions on medium-mass nuclei. The bombarding energy is a few times that of the Coulomb barrier. The Coulomb barrier for proton (B) is labeled on the abscissa. [Lil01]..... 5
1.4 Relationship between cross-section and the increase in the incident alpha particle energy [Kra88]..... 6
1.5 Energy levels populated by a (p,2n) reaction[Mor76]..... 7
1.6 γ-spectra due to the reaction ^{208}Pb + p at three different proton energies; namely 7.5 MeV, 10.5 MeV and 12.5 MeV. Increasing the proton energy favours the formation of ^{207}Bi but at the expense of high background (as depicted in E_p = 12.5 MeV. [Pro70])..... 8
1.7 γ-spectra due to the formation of the ^{207}Bi from ^{208}Pb and ^{207}Bi at proton energies of 15 MeV and 10.5 MeV respectively. [Pro70]..... 9
1.8 The γγ-coincidence spectrum of in ^{208}Bi following electron capture of ^{208}Po using a 7.6 cm x 7.6 cm gating NaI(Tl) detector. The gate was set at the 291.1 keV peak. [Hag69]..... 10

2.1 The Photoelectric Effect [Fags]..... 13
2.2 The Compton Scattering [The97]..... 14
2.3 Pair Production [Gif96]..... 15
2.4 Plan-view of the iThemba LABS facilities..... 17
2.5 AFRODITE Clover Detector array..... 19
2.6 A clover detector with tapered rectangular cryostat and a cylindrical liquid nitrogen dewar [Mab03]..... 20
2.7 A BGO Compton suppression shield [Mab03]..... 22
2.8 (a) Compton suppressed and unsuppressed γ-spectra from a ^{60}Co radioactive source. (b) Compton Suppression Factor (CSF) found from the ratio of the unsuppressed to the suppressed spectra. The CSF is about 1.4. [Mab03]..... 23
2.9 The AFRODITE Array Electronics..... 26

3.1 Schematic step-by-step representation of the processes followed during data analysis..... 29
3.2 (A)Total projection of a matrix for the energy range $0 < E_\gamma < 1500$keV at beam energy of 11.6MeV..... 30
(B)Total projection of a matrix for the energy range $1000\text{keV} < E_\gamma < 15000$KeV at beam energy of 11.6 MeV..... 30
3.3 (A)Total projection of a matrix for the energy range $0 < E_\gamma < 1500$keV at beam energy of 11.9 MeV..... 31
(B) Total projection of a matrix for the energy range $1000\text{keV} < E_\gamma < 15000$keV at beam energy of 11.9 MeV..... 31
3.4 (A)Total projection of a matrix for the energy range $0 < E_\gamma < 1500$keV at beam energy of 13.2 MeV..... 32
(B) Total projection of a matrix for the energy range $1000\text{keV} < E_\gamma < 15000$KeV at energy of 13.2 MeV..... 32
3.5 (A)Total projection of a matrix for the energy range $0 < E_\gamma < 1500$keV at beam energy of 14.8MeV..... 33
(B) Total projection of a matrix for the energy range $1000\text{keV} < E_\gamma < 15000$KeV at energy of 14.8MeV..... 33
3.6 The relative efficiency for the 8 Clover and 8 LEPS detectors measured with ^{152}Eu

(filled-circles) and ^{133}Ba (open circles) radioactive sources placed on the target ladder at the target position [Mab02] 35

4.1 Partial level decay scheme of ^{208}Bi from the transitions shown in figures 4.2 – 4.6 [Kau04] 40
4.2 Single coincidence γ-ray spectra gated on the 538.5 keV ^{208}Bi γ-ray transition for the 11.6MeV (A) and 11.9MeV (B) beam energy 41
Single coincidence γ-ray spectra gated on the 538.5 keV ^{208}Bi γ-ray transition for the 13.2MeV (C) and 14.8MeV (D) beam energy 42
4.3 Single coincidence γ-ray spectra gated on the 570.1 keV ^{208}Bi γ-ray transition for the 11.6MeV (A) and 11.9MeV (B) beam energy 43
Single coincidence γ-ray spectra gated on the 570.1 keV ^{208}Bi γ-ray transition for the 13.2MeV (C) and 14.8MeV (D) beam energy 44
4.4 Single coincidence γ-ray spectra gated on the 603.3 keV ^{208}Bi γ-ray transition for the 11.6MeV (A) and 11.9MeV (B) beam energy 45
Single coincidence γ-ray spectra gated on the 603.3 keV ^{208}Bi γ-ray transition for the 13.2MeV (C) and 14.8MeV (D) beam energy 46
4.5 Single coincidence γ-ray spectra gated on the 873.3 keV ^{208}Bi γ-ray transition for the 11.6MeV (A) and 11.9MeV (B) beam energy 47
Single coincidence γ-ray spectra gated on the 873.3 keV ^{208}Bi γ-ray transition for the 13.2MeV (C) and 14.8MeV (D) beam energy 48
4.6 Single coincidence γ-ray spectra gated on the 906.2 keV ^{208}Bi γ-ray transition for the 11.6MeV (A) and 11.9MeV (B) beam energy 49
Single coincidence γ-ray spectra gated on the 906.2 keV ^{208}Bi γ-ray transition for the 13.2MeV (C) and 14.8MeV (D) beam energy 50
4.7 Excitation functions for the reaction product, ^{208}Bi, for (a) 538.5 keV and (b) 570.1 keV transitions 52
Excitation functions for the reaction product, ^{208}Bi, for (c) 601.8 keV, (d) 873.3 keV and (e) 906.2 keV transitions 53
4.8 (A) Partial level decay scheme of ^{207}Bi from the transitions depicted in figures 4.9 – 4.12[Sch71] 55
(B) Partial level decay scheme of ^{207}Bi from the transitions depicted in figures 4.9 – 4.12[Sch71] 56
4.9 Coincidence γ-ray spectra gated on the 405.8 keV ^{207}Bi γ-ray transition which shows a coincidence relationship with the 742.6 keV transition 57
4.10 Coincidence γ-ray spectra gated on the 629.8 keV ^{207}Bi γ-ray transition. The 629.8 keV gate exhibits a coincidence relationship with the 742.6 keV transition 58
4.11 Coincidence γ-ray spectra gated on the 669.6 keV ^{207}Bi γ-ray transition 58
4.12 Coincidence γ-ray spectra gated on the 742.6 keV ^{207}Bi γ-ray transition. The 742.6 keV gate exhibits a coincidence relationship with the 629.8 keV transition 59
4.13 Excitation functions for the reaction product, ^{207}Bi, for (a) 405.8 keV 60
4.13 Excitation functions for the reaction product, ^{207}Bi, for (b) 629.8 keV 61
4.13 Excitation functions for the reaction product, ^{207}Bi, for (c) 669.6 keV 61
4.13 Excitation functions for the reaction product, ^{207}Bi, for (d) 742.6 keV 62
4.14 Excitation functions for the sum of the 4^+ ^{208}Bi and the $(9/2)^-$ ^{207}Bi ground state transitions as a function of beam energy 64
4.15 Excitation functions for the ^{208}Bi(906.2 keV) and ^{207}Bi(669.6 keV) 65

List of Tables

2.1 Layout of iThemba LABS SSC accelerator facility..... 18
2.2 Electronic modules used in an AFRODITE Array..... 27

4.1 The level energies E_γ, absolute intensities (I) and spin assignments at four beam energies for the ^{208}Bi nuclei..... 51
4.2 Excitation functions for the ^{208}Bi residual nuclei normalised to the 601.8 keV transition..... 54
4.3 The level energies E_γ, absolute intensities (I) and spin assignments at four beam energies for the ^{207}Bi nuclei..... 60
4.4 Excitation functions for the ^{207}Bi residual nuclei normalised to the 742.6 keV transition..... 62

Chapter 1

Introduction

1.1 Overview

There is distinct relationship between the incident proton energy and the amount/intensity of the gamma rays emitted during the nuclear reactions between $^{208}Pb(p,n\gamma)$ ^{208}Bi and $^{208}Pb(p,2n)^{207}Bi$. Unlike the odd-odd nuclei, a (p, n) reaction on an even-even nucleus (^{208}Pb) yields fewer transitions associated with low-lying levels of limited excitation energy and spin. If two gamma rays have the same excitation function, then their origin should be the same. The intensities of the gamma rays emitted will indicate the effect of the incident energy on the production of the residual ^{208}Bi and ^{207}Bi nuclei.

This paper examines the intensity of known gamma rays in the reactions $^{208}Pb(p,n\gamma)$ ^{208}Bi and $^{208}Pb(p,2n\gamma)^{207}Bi$ at four incident proton energies; namely 11.6 MeV, 11.9 MeV, 13.2 MeV and 14.8 MeV, as a function of bombarding energy. The γ-rays are detected with 6 Clover detectors of the AFRODITE array, implying that only high-energy gamma rays having energy range 0.4 MeV and 2 MeV are considered.

1.2 Compound nuclear reactions overview

When an incident particle like a proton or a neutron has an impact parameter smaller than the target nuclear radius, it will enter the target nucleus, and it will interact with one of the nucleons of the target through a simple scattering process. The positive energy projectile becomes momentarily trapped in one of the nucleus' single particle virtual states as depicted in fig 1.1.

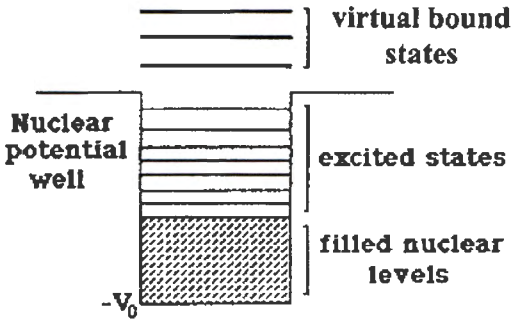

Figure 1.1: *Bound states in square well [She03]*

Through successive interactions of the particle and the nucleons, the energy of the particle is continuously shared among the nucleons, raising some of the nucleons' energies and itself dropping into one of these states due to energy loss. This average increase in the energy of the nucleon is not enough to free it from the nucleus, but due to successive random collisions, there is a statistical energy distribution such that there is a probability that a single nucleon will gain enough energy to escape from the nucleus. The result is the formation of an intermediate, many particle excited state, after the incident particle has been absorbed before the emission of the outgoing particle(s). The compound nucleus formation process of this nature is depicted in figure 1.2.

This intermediate, many particle state is referred to as the compound nucleus. The reaction between a projectile **a** and target **X** via the compound nucleus formation can be represented by the equation:

$$a + X \longrightarrow {}^*C \longrightarrow b + Y \qquad (1.1)$$

where $^*C$ denotes the many particle, excited state - the compound nucleus.

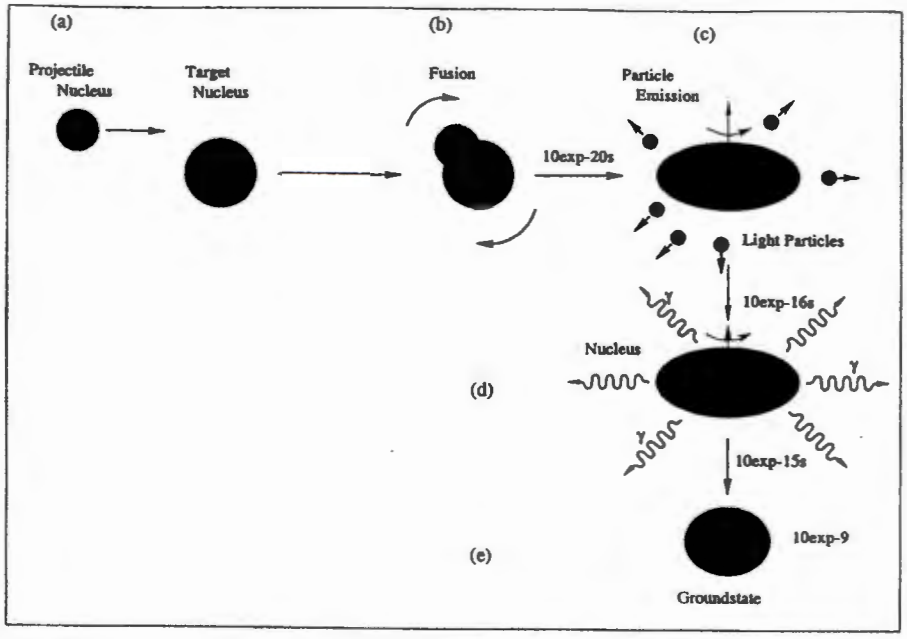

Figure 1.2: *Stages in the compound nucleus formation process [Mab02]*

The compound nuclear reaction is considered to proceed via two independent stages:

i. The formation of the compound nucleus; and

ii. De-excitation and decay of the compound nucleus.

At proton energies between 11 MeV and 15 MeV, the (p,n) reaction from ^{208}Pb to ^{208}Bi proceed via the compound-nucleus formation. The characteristic nuclear reaction can be written as:

$$^{208}\text{Pb} + \text{p} \longrightarrow {}^{209}\text{Bi}^* \longrightarrow {}^{208}\text{Bi} + \text{n}\gamma \qquad (1.2)$$

where ^{209}Bi* is the intermediate compound nucleus formed during ^{208}Bi formation.

G.B. Hansen et al [Han63] identified three independent steps that the (p,2n) reactions follow:

a) a compound nucleus formation in an excited state of say Q_1 MeV

b) formation of an intermediate nucleus after the evaporation of one neutron, which is excited to about Q_2 MeV; and

c) the evaporation of the second neutron, leading to a residual nucleus excited to about Q_3 MeV,

where $Q_1 > Q_2 > Q_3$

The complete process can be represented by the following reaction:

$$^{208}Pb + p \longrightarrow {}^{209}Bi^* \longrightarrow {}^{208}Bi^* + n\gamma \longrightarrow {}^{207}Bi + n\gamma \qquad (1.3)$$

$$Q_1 > Q_2 > Q_3$$

Further studies on the (p,2n) reactions were conducted by Sakai et al [Sak65] using 12, 13 and 14 MeV protons on Rh, Sb, I, Cs, Re, Ir and Au isotopes.

The following characteristics of the compound-nucleus reactions between the small projectile and the larger target nucleus are worth noting:

- This model works best for low incident energies of between 10 MeV – 20 MeV [Krane88]. This is because of the small probability that the incident particle will escape from the nucleus with its original identity and its energy intact.
- The angular distribution of the products formed is the same in all directions. This is mainly due to the random collisions among the nucleons.
- The more energy is given to the compound nuclei, the more likelihood of more particles 'evaporating' i.e. leaving the nucleus due to high energy absorbed during collisions. The Coulomb barrier hinders the emission of protons from the compound nucleus. Figure 1.3 shows the energy spectra of the emitted protons and neutrons from proton induced reactions on medium-mass nuclei. Therefore a compound nucleus having sufficient energy to emit one or two particles will most likely emit a neutron rather than a charged particle. In the case of a highly neutron deficient compound nucleus, more energy will be required to remove a neutron than

- a proton from a compound nucleus. Neutrons never experience a Coulomb barrier, protons always do.
- From the cross-section vs. incident energy of the alpha particle relation, each cross-section exhibit a Gaussian-like shape as shown in figure 1.4.

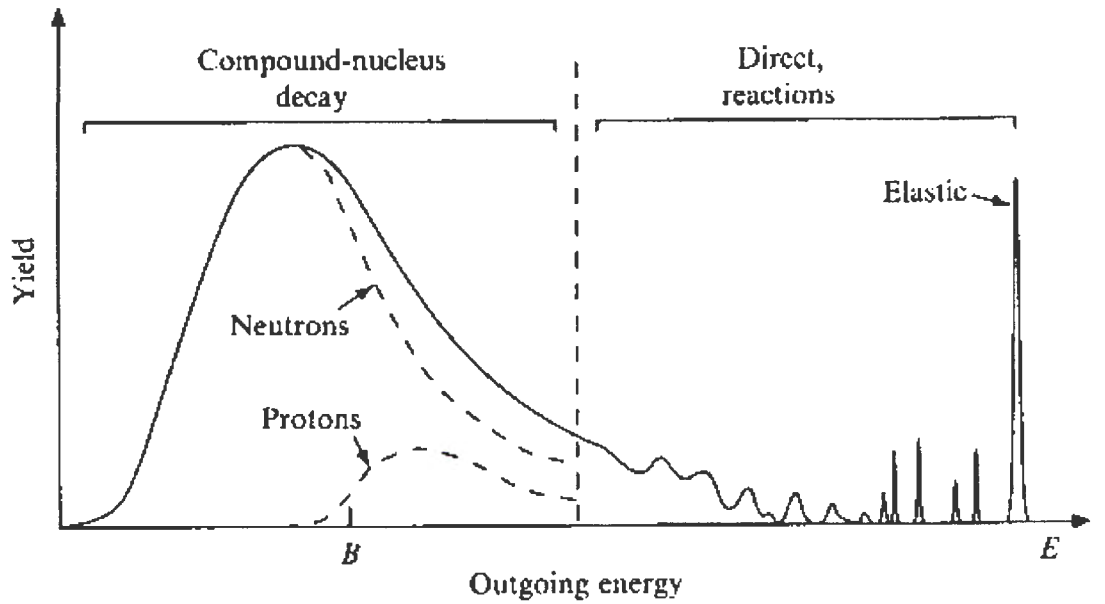

Figure 1.3: *Energy spectra of protons and neutrons emitted from proton induced reactions on medium-mass nuclei. The bombarding energy is a few times that of the Coulomb barrier. The Coulomb barrier for proton is labeled on the abscissa. [Lil01]*

As a result, the formation of a given compound nucleus may be due to many different reactions, but the probability of populating a final state of the residual nucleus is independent on the formation process of the compound nucleus, and depends only on the amount of the excitation energy available. This is referred to as the independence hypothesis of Niels Bohr [Kra88].

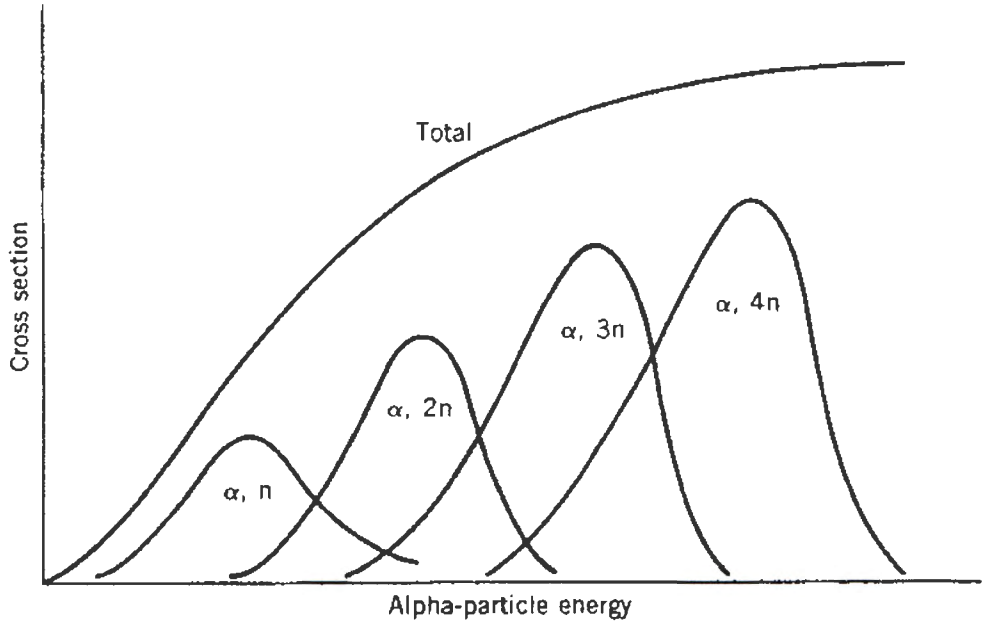

Figure 1.4: *In each reaction, there is an increase in the cross-section to the maximum followed by a decrease, as the incident energy is increased. This increases the probabilities of an additional neutron to be emitted. This is analogous to the (p,xn) reaction, where x = 1,2,3,4,.... [Kra88]*

1.3 Previous studies

The compound nucleus formation model assumes that "the relative probability for the decay into any specific set of products is independent of the means of formation of the compound nucleus"[Krane88]. The total energy given to the system will determine the decay probabilities (discussed in section 1.2 above).

According to [Mor76], compound nuclear reactions involving one particle and subsequent gamma-ray emission, that is, (p, nγ), (p, p'γ) and (n, n'γ), are important in determining the population of levels that were occupied by the outgoing particle. The measurement of the intensity of the gamma rays due to compound nuclear reactions gives the population of levels reached by the outgoing particle. Changing the intensities of the incident bombarding particles and observing the gamma-ray intensities, transitions can be correctly assigned. Proton-induced reactions like (p,n) and (p,2n) are characterized by low angular momentum

transfer. A 14 MeV proton impinging on a heavy nucleus will induce predominantly (p,2n) reactions. This is illustrated in figure 1.5. Because of the low incident proton energy, the final nuclear energy state is bound to be fairly low.

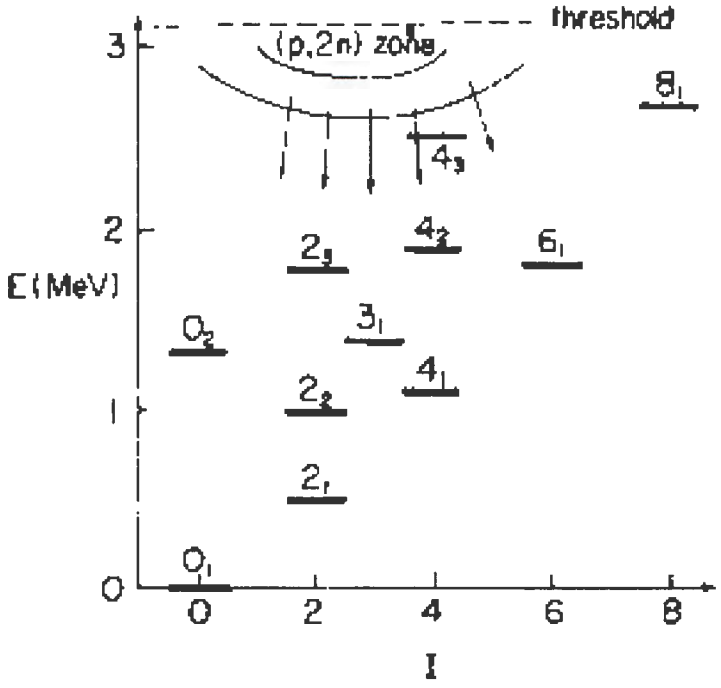

Figure 1.5: *Energy levels populated by a (p,2n) reaction. The excitation functions show the sensitivity of the populations with the proton energy and energy levels. [Mor76]*

The experiment to determine the decay scheme of the ^{208}Bi nucleus from the reaction ^{208}Pb(p,nγ) ^{208}Bi at incident proton energies between 7.0 MeV and 12.5 MeV was published by Proetel et al., [Pro70]. More than 100 γ-ray transitions were identified. At these bombarding energies, the reactions were mainly via compound nucleus formation and the reaction cross sections were fairly large. At incident proton energies higher than 10.5 MeV, ^{208}Bi γ-rays were obscured in the spectra by peaks from the other reaction channels. This is

depicted in figure 1.6 and 1.7 [Pro70]. This resulted in the measurement of the gamma ray intensities not being accurate.

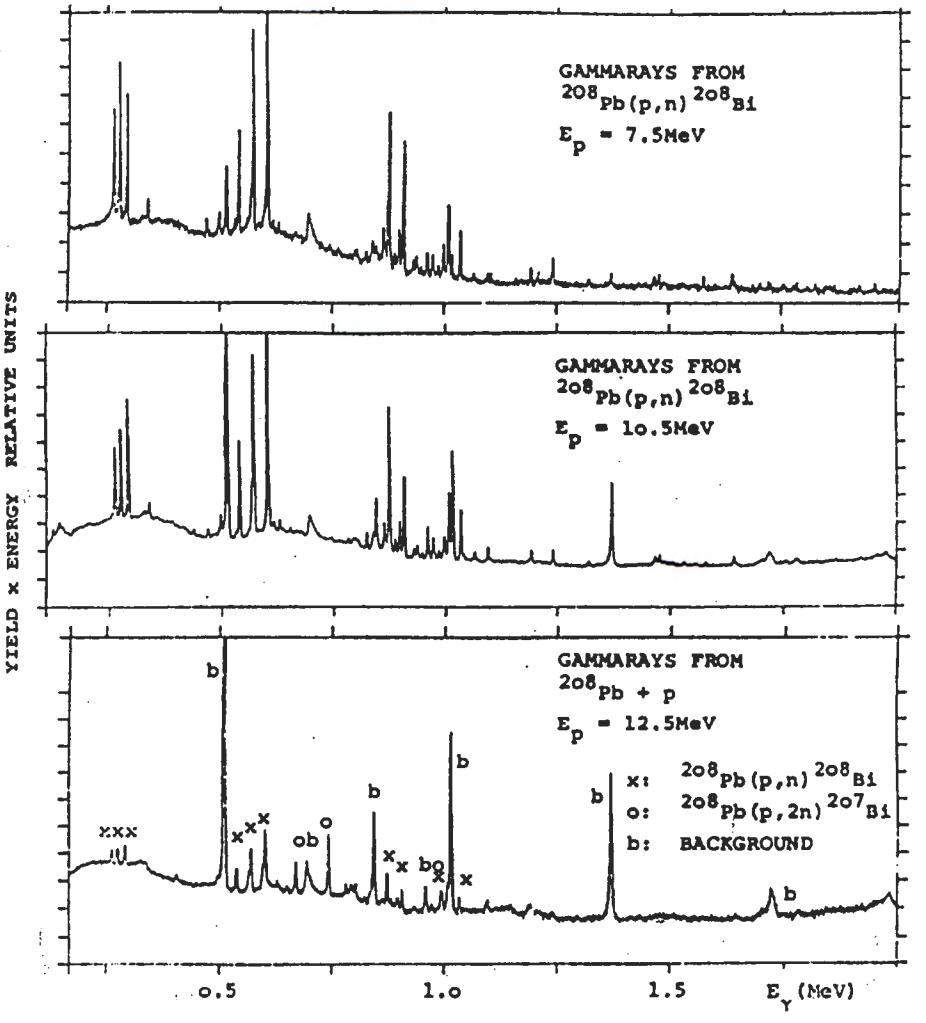

Figure 1.6: *γ-spectra due to the reaction ^{208}Pb + p at three different proton energies; namely 7.5 MeV, 10.5 MeV and 12.5 MeV. Increasing the proton energy favours the formation of ^{207}Bi but at the expense of high background (as depicted in E_p = 12.5 MeV). [Pro70]*

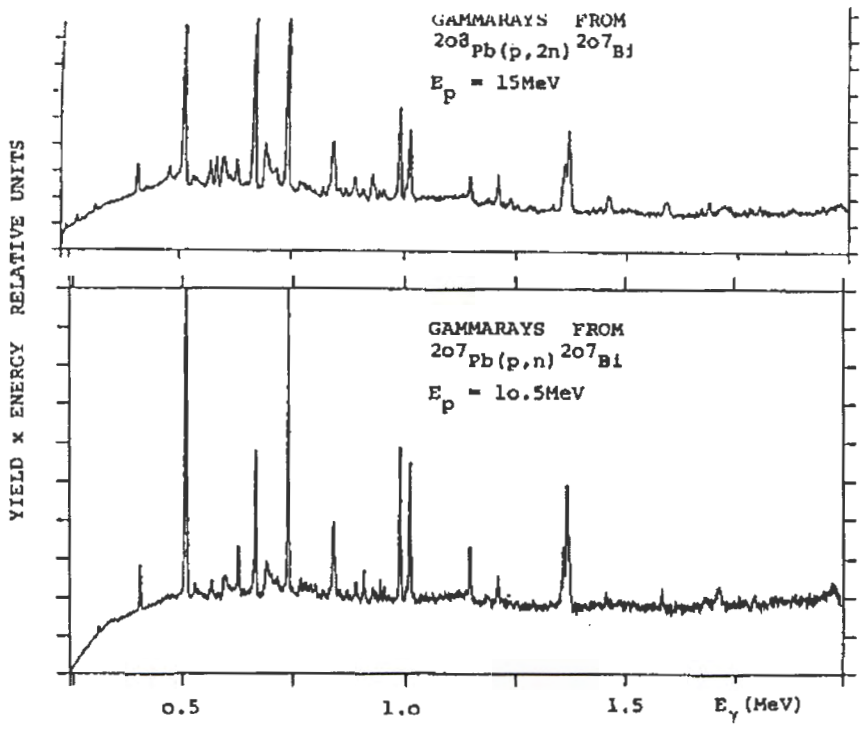

Figure 1.7: *γ-spectra due to the formation of ^{207}Bi from ^{208}Pb and ^{207}Bi at proton energies of 15 MeV and 10.5 MeV respectively. [Pro70]*

Further experiments to obtain the transitions and intensities in ^{208}Bi were conducted by M. Bonitz et al [Bon68] from ^{208}Pb(d,2n)^{208}Bi. Gabsdil [Gab68] studied the decay of the ^{208m}Bi from a (γ,n) reaction using small Ge(Li) detectors. The energy and intensity errors were relatively high, thus requiring the need for improvement.

G.B. Hansen et al [Han63] studied proton-induced reactions at proton energies between 8 and 12 MeV by means of a magnetic spectrometer. Erskine [Ers64] studied the level structure and excited states of ^{208}Bi with the high-resolution magnetic spectrograph with the ^{209}Bi(*d*,t)^{208}Bi reaction at a bombarding energy of 12 MeV. Due to poor resolution of the magnetic spectrometer as compared to solid-state detectors, energy measurements were not accurate. Hagee et al [Hag69] measured the transitions and the relative intensities of the γ-ray photons in the ^{208}Bi from the electron capture decay of ^{208}Po using Ge(Li) detector for the

high-energy γ-rays and Si(Li) detector for low-energy γ-rays. From their experiment, the only γ-rays considered were those in coincidence with the 291.9 keV photon, namely, 539.1 keV, 570.7 keV and 602.9 keV. The gating detector used in the γγ-coincidence spectrum was a 7.6 cm x 7.6 cm NaI(Tl) detector. This is indicated in figure 1.8, where the coincidence of the 291.9 keV line with the 539.1 keV, 570.7 keV and 602.9 keV γ-rays can be explicitly seen. The 12 cm^3 Ge(Li) detector was used to perform the analysis. However, their results were limited to 925.6 keV and 634.4 keV levels in ^{208}Bi. No new transitions in ^{208}Bi were found.

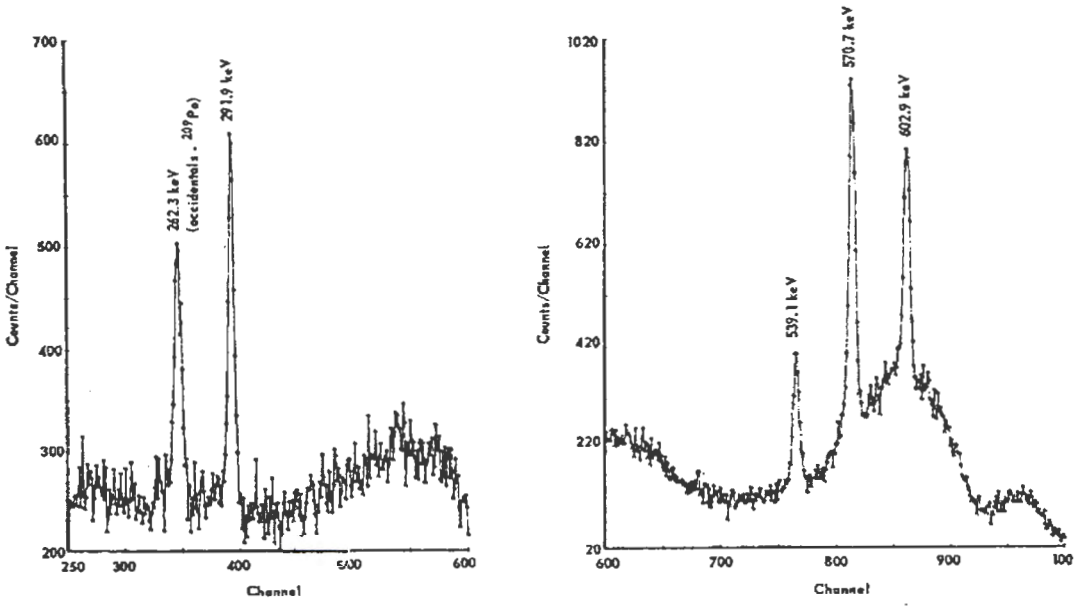

Figure 1.8: *The γγ-coincidence spectrum of ^{208}Po using a 7.6 cm x 7.6 cm gating NaI(Tl) detector. The gate was set at the 291.9 keV peak. The gating transition at 291.9 keV reappears on the spectra due to poor energy resolution of the NaI(Tl) detectors. [Hag69]*

Gloris et al [Glo01] used γ-spectrometric techniques to measure the excitation functions for the proton induced production of residual nuclides from lead at intermediate energies i.e. proton energies between 64.8 MeV and 2.6 GeV. At these energies, about 2000 individual cross-sections from 127 reactions were determined. Because of the higher proton energies, excitation functions exhibited reaction modes like multi-fragmentation, instead of the compound nucleus formation and the subsequent evaporation of neutrons from lead.

1.4 Aim of this study

The emission of gamma rays by radioactive sources plays a primary role in the study of the excited nuclear states. Amongst other wide variety of applications, gamma-ray spectroscopy can be applied in astro- and cosmo- physics, medicine, space and aviation technology to accelerator-based nuclear waste transmutation and energy amplification [Glo01]. Heavy elements like Pb and Bi are considered as spallation- target materials in accelerator-based experiments such as those involving waste transmutation and energy amplification. They are also useful as targets in spallation neutron sources. Gamma-ray spectroscopy is the most precise and often easiest way of obtaining information about the locations of excited states, which are important for calculations based on any nuclear model. On the other hand, "gamma energy measurements are also useful for separating doublets and multiplets which were not separated by the analysis of the particle spectra" [Mor76]. The use of the solid-state detectors in the gamma energy measurements usually yields more accurate results compared to energy measurements with the magnetic spectrographs. The use of the AFRODITE array (discussed in section 2.2.3) will enable the analysis with good resolution as well as determining more accurately the relationship between the incident proton energy on ^{208}Pb and the intensity of the gamma rays emitted in the decay of excited states in ^{208}Bi and ^{207}Bi nuclei.

The aim of this paper is to study the relationship between the incident proton energy and the intensity of the previously known gamma-rays emitted in the reactions ^{208}Pb(p,nγ) ^{208}Bi and ^{208}Pb(p,2n)^{207}Bi. Four incident proton energies considered are: 11.6 MeV, 11.9 MeV, 13.2 MeV and 14.8 MeV. These high-energy gamma rays were detected with the 6 AFRODITE clover detectors [New98]. In previous measurements of the gamma ray spectra at low incident energies, detection of gamma rays of energy greater than 10 MeV was marred by poor resolution of the NaI detectors [Pro70]. Similarly, small Germanium detectors failed to yield good results at these energies. Therefore the use of the Clover detectors is suitable for the detection of the high-energy γ-rays, which were previously not accurately detected. Large volume of the clover detectors makes AFRODITE array suitable for measuring such high-energy gamma rays.

Chapter 2

Experimental Techniques and Equipment

In this experiment, the low energy proton beam was directed at the ^{208}Pb target, thereby inducing the (p,n) and (p, 2n) reactions to yield ^{208}Bi and ^{207}Bi, respectively. The ^{208}Bi and ^{207}Bi formed were identified by the characteristic gamma rays emitted during their de-excitation. These gamma rays were detected using 6 AFRODITE clover detectors, which were operated in positive output polarity mode to enable the energy detection range to be increased to 20 MeV. This chapter outlines the experimental equipment employed in this study, target requirements, the detection of the gamma rays, and subsequently their energies.

2.1 Interaction of γ-rays with matter

Gamma rays interact with matter in a number of possible ways. In order to determine and measure the gamma radiation emitted following the compound nucleus decay as discussed in section 1.2 above, the process by which gamma rays interact with matter, and hence the detector material, becomes important. In the energy range of $100\text{keV} < h\nu < 30$ MeV, there are three dominating interaction processes (discussed in section 2.1.1 below), by which gamma rays interact with matter; namely the Photoelectric Effect, Compton Scattering, and Pair Production.

2.1.1 Photoelectric Effect

The process of photoelectric absorption is shown in figure 2.1. An incident photon is completely absorbed by an atom in the absorber material, and one of the atomic electrons, the photoelectron, is ejected.

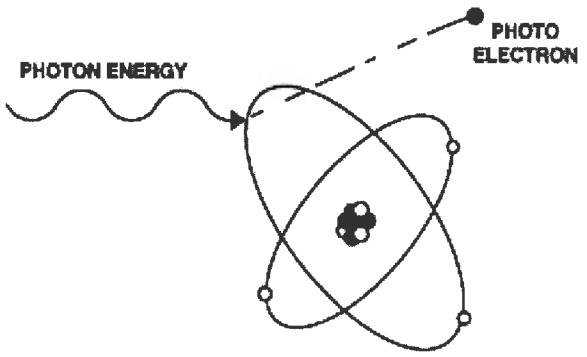

Figure 2.1: *The Photoelectric Effect [Fags]*

The electron must be bound to the atom, to conserve energy and momentum. The ejected electron has kinetic energy given by:

$$E_e = E_\gamma - B_e \tag{2.1}$$

where B_e is the binding energy of the atomic electron. The vacancy left in the atomic structure by the ejected electron is filled by one of the electrons from a higher shell. This transition is accompanied by an emission of an X-ray or Auger electrons. The detector also absorbs these X-rays. Photoelectric absorption is the most favourable process for the γ-ray spectroscopy, since the incident photon deposits all of its energy into the detector, but it is only dominant for low energy photons (< 200 keV).

The interaction is again dependent upon atomic number Z. An approximate expression for the absorption probability σ is

$$\sigma \alpha Z^n \tag{2.2}$$

Here n is normally between 4 and 5 depending on the absorber material. This dependence on the atomic number Z explains the choice of high-Z materials such as lead for shielding purposes.

2.1.2 The Compton Scattering

During Compton Scattering, an incident photon with energy $E_{\gamma 0}$ impinges on an electron in matter, thereby scattering it off (figure 2.2). In this process, part of the photon energy is transferred to the electron. The excited electron is ejected or moved into an excited atomic state.

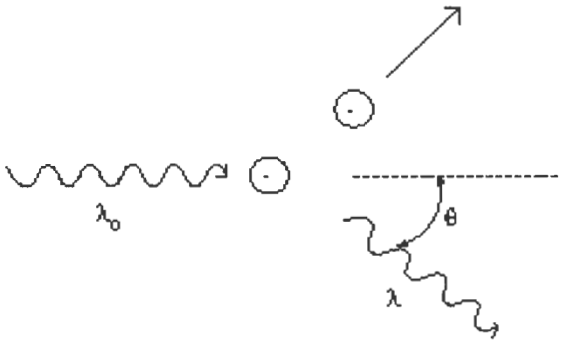

Figure 2.2: *The Compton Scattering [The97]*

The scattered gamma rays will have longer wavelength than the incident photon and hence, reduced energy. The shift of the wavelength increased with scattering angle according to the Compton formula

$$\lambda = h/m_e c(1-\cos\theta), \tag{2.3}$$

where θ is the scattering angle and the quantity $h/m_e c$ is called the Compton wavelength. From the energy and momentum conservation, the initial energy ($E_{\lambda 0}$) and final energy (E'_{λ}) of the gamma ray photon are related by:

$$E'_{\lambda} = E_{\lambda 0} / 1 + E_{\lambda}/m_e c^2 (1-\cos\theta), \tag{2.4}$$

where $m_e c^2$ (= 511 keV) is the rest mass energy of the electron. From equation 2.4, maximum energy transfer to the electron occurs at $\theta = 180^0$. This process is dominant within the energy range of (200 – 1000) keV, and becomes ineffective as the energy increases.

2.1.3 Pair Production

Pair production is the formation of two β-particles, one positive (positron) and the other negative (electron) from a photon energy traveling through matter, usually in the vicinity of the Coulomb field of an atom (figure 2.3). It is a direct conversion of radiant energy to matter. For pair production to occur, the photon energy must be at least equivalent to the mass of two electrons or positrons.

Therefore to produce an electron-positron pair, the "threshold" required photon energy must be at least 1.022 MeV (2 x 0.511 keV). Excess photon energy over the "threshold" is converted into the kinetic energy of the electron-positron pair. Both the electron and the positron formed will be slowed down, prompting the annihilation process, whereby the positron will disappear by conversion into photons. This will occur when the positron interacts with an electron to produce two gamma rays of energy 511 keV. This process predominates at high energies.

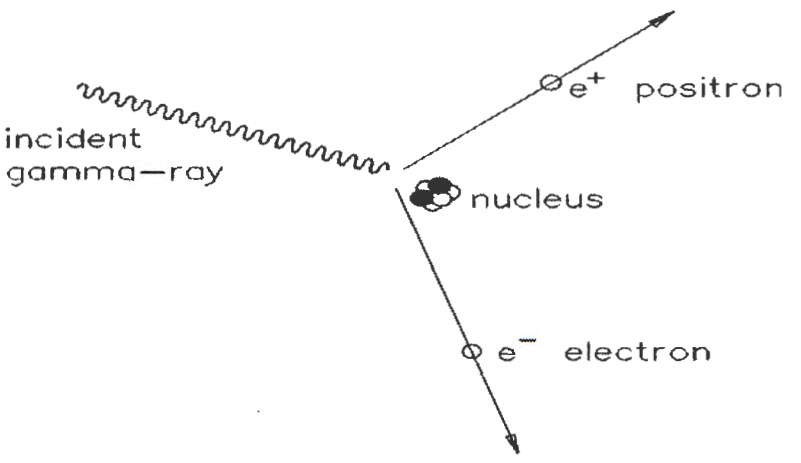

Figure 2.3: *Pair Production [Gif96]*

The absorption probability for pair production is given by:

$$\sigma \alpha Z^2 I, \tag{2.5}$$

where Z is the atomic number of the target material.

2.2 Experimental Equipment

The following pieces of equipment are used to study the excitation functions of the reactions $^{208}Pb(p, n)^{208}Bi$ and $^{208}Pb(p, 2n)^{207}Bi$:

- The accelerator producing the required accelerated particles (beam energy);
- Beam lines that direct the beam to the target;
- Necessary reactions that produce nuclei of interest;
- γ-ray detectors with high efficiency and good resolution;
- Electronics; and
- Data Acquisition and Computing systems.

2.2.1 The facilities at iThemba LABS

The experiment described herein was performed at iThemba Laboratories for Accelerator Based Sciences (LABS), situated at Faure in the Western Cape, South Africa. iThemba LABS is a multidisciplinary research and training institution for basic and applied research using particle beams, particle radiotherapy for the treatment of cancer and radio-isotope production for nuclear medicine and research.

The experiment was performed using a proton beam delivered by the large Separated-Sector Cyclotron (SSC), which is capable of accelerating heavy ions to high energies. A layout of iThemba LABS is shown in figure 2.4.

2.2.2 Separated-Sector Cyclotron (SSC)

Activities are based around four sub-atomic particle accelerators. The large k=200 separated sector cyclotron, having dimensions of 13.2 MeV m in diameter and 7 m in height, accelerates protons to maximum energies of about 200 MeV, and heavier particles to much higher energies. It has four sector magnets, positioned to an accuracy of one tenth-of a

millimeter and having total weight of 140 tonnes. Charged particles to be accelerated are fed to it via one of two smaller injector cyclotrons. The first injector cyclotron (SPC1) provides intense beams of light ions, usually protons, for radioisotope production and radiotherapy. The second injector cyclotron (SPC2), used in this experiment, provides beams of polarized light ions such as proton and deuteron, or heavy ions such as krypton, iodine or carbon.

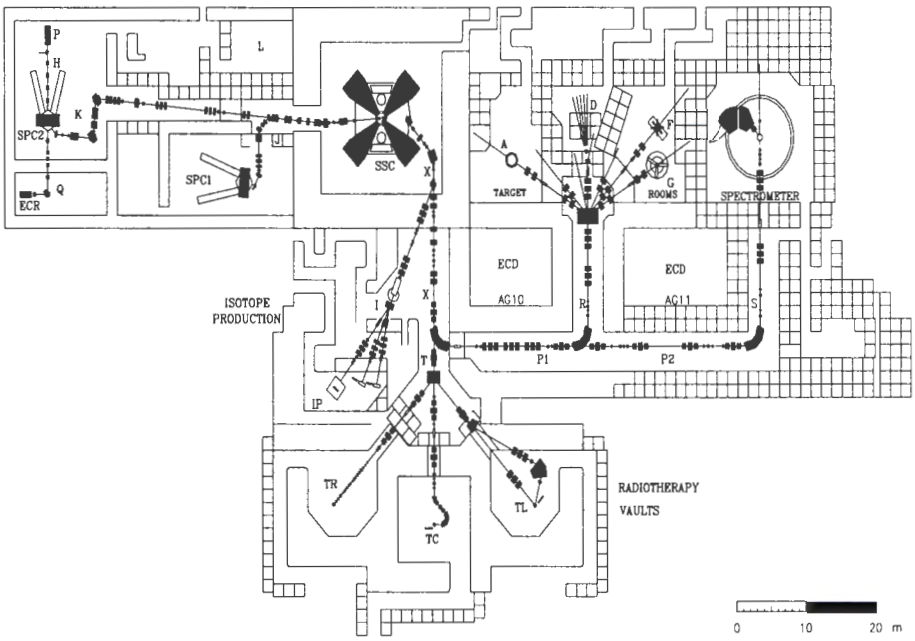

Figure 2.4: *Plan-view of the iThemba LABS facilities (see Table1)*

Labels	Description
A	Scattering chamber beam line
D	Collimated neutron beam facility
ECR	Electron Cyclotron Resonance (ECR) ion source
ECD	Electronic and cable distribution
F	High-energy gamma-ray detectors (AFRODITE array)
G	Gamma-ray angular correlation table
IP	Isotope production facility
L	Low-energy experimental area
P	Polarised-ion source
SPC1	Solid-pole injector cyclotron for light ions
SPC2	Solid-ion cyclotron for heavy and polarized ions
SSC	Separated-Sector Cyclotron
TC	Isocentric system for neutron therapy
TR	Horizontal beam line for proton therapy
TL	Beam lines for proton

Table 2.1: *Layout of iThemba LABS SSC accelerator facility*

2.2.3 AFRODITE Array

When a gamma ray from a radioactive source interacts with matter, there are three primary methods by which it is absorbed. They are the Photoelectric Effect, the Compton Interaction and Pair Production (discussed in section 2.1). AFRODITE, an acronym for AFRican Omnipurpose Detector for Innovative Techniques and Experiments [New98], is a spectrometer used to detect both high and low energy photons (X- and γ-rays) with high efficiency (see figure 2.5). To achieve this, the rhombicuboctahedron shaped frame, with 16

detector positions, combines two sets of High Purity Germanium (HPGe) γ-ray detectors, namely, the 8 Clover detectors and 8 Low Energy Photon Spectrometers

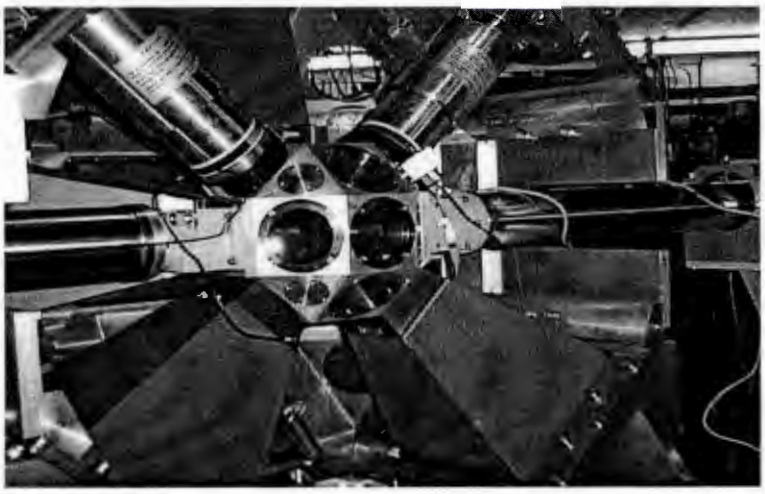

Figure 2.5: *AFRODITE clover detector array*

(LEPS) for photons between 30 and 300 keV. There are 16 square facets at 45, 90 and 135 degrees with respect to the beam line. The top most square facet, positioned at 90^0 with respect to the beam line, is used to support the hydraulic target positioner. The other 15 square facets are used to mount the detectors. The Clover detectors are surrounded by a Compton-suppression shield, bismuth germanate $Bi_4Ge_3O_{12}$ (BGO), a highly efficient scintillator that detects gamma rays that are Compton scattered (discussed in section 2.2.5). This enhances a better full-energy to partial-energy events ratio – called the peak-to-total or P/T ratio.

Another important factor required by the detectors designed to measure the energy of radiation is the energy resolution of the detector. This is the extent to which the detector can distinguish between two γ-rays whose energies lie close to each other. It can be quantified by supplying a monoenergetic beam of radiation into the detector, and thereafter measure the FULL WIDTH at HALF MAXIMUM (FWHM) of the peak. This width occurs due to the fluctuations in the number of excitations and ionizations produced. Energies closer to the FWHM interval are regarded as noise and unresolvable. The relative resolution at a given energy E is given by $\delta E/E$ (usually expressed as a percentage), where δE is the change in energy. The relative resolution for the Clovers is about 0.1%.

2.2.4 Clover detectors

Clover detectors are ideal for detecting high-energy gamma rays because of their high efficiency in the add-back mode. It consists of four n-type coaxial HPGe crystals having crystals spacing of about 0.2 mm apart [Jon95]. The crystals with the dimensions; 70 mm in length, 50 mm in diameter, 36 mm tapering length and 50 mm surface diagonal length, are housed in the same cryostat. The front of the crystals are tapered in order to achieve maximum close packing [Jon95]. Each crystal act independently from the others, with its own electronics.

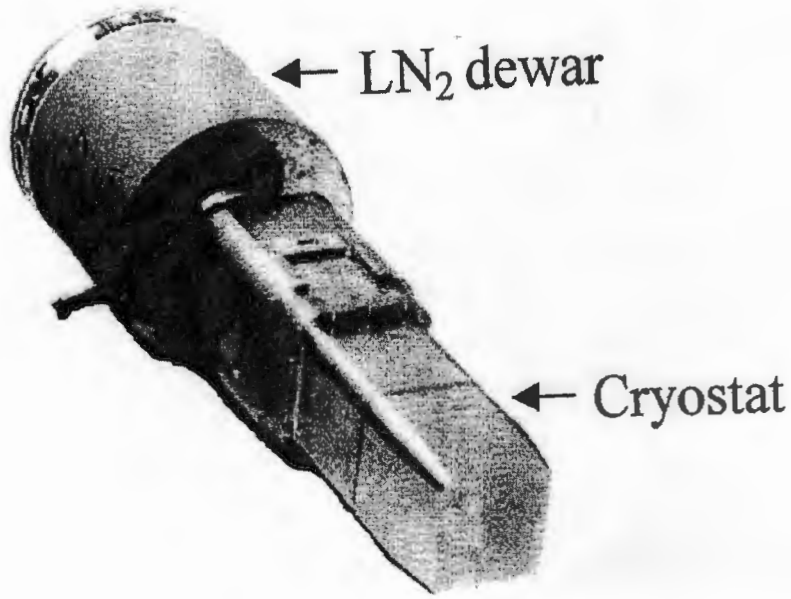

Figure 2.6: *A clover detector with tapered rectangular cryostat and a cylindrical liquid nitrogen (LN_2) dewar [Mab03].*

The granularity of the clover detectors results in a decreased Doppler broadening of the peaks and allows the possibility of the reconstruction of the total γ-energy by adding up energies deposited in one or more crystals due to Compton scattering (add-back), which thus increases the photo peak efficiency [New98]. The Clover detectors are coupled to an

automatic LN_2 filling system, which fills the dewars with LN_2 from the storage tank every 12 hours (figure 2.6).

The total photo-peak efficiency of the AFRODITE array at 1MeV gamma-ray energy is estimated to be about 1.6%.

Other notable technical specifications of the AFRODITE array include [New98]:

- The distance from the crystal surface to the target center, D_{tc} = 196 *mm*.
- The distance from the detector end-cap to the crystal surface, D_{ec} = 20 *mm*.
- The total opening angle, T_{ang} = 23.2^0
- The solid angle per detector, S_{ang} = 1.34 % of 4π (for a distance of 0.2 mm between crystals).

2.2.5 Compton Suppression

The reduction of the unwanted γ-ray Compton background is referred to as Compton suppression. This is achieved by employing the bismuth germanate $Bi_4Ge_3O_{12}$ (BGO) Compton suppression shields (≈ 26 cm in length), which house the Clovers (shown if figure 2.7).

Suppressed and unsuppressed spectra were obtained with a ^{60}Co radioactive source. Compton scattered γ-ray events from the germanium crystal are vetoed by the BGO shield, yielding a suppressed spectrum, whereas the unsuppressed spectrum contains all the γ-rays detected by the Clover, whether scattered or not into the BGO shields. The normalization of both the suppressed and unsuppressed spectra is done such that the number of counts in the photo-peaks recorded is the same [Mab03].

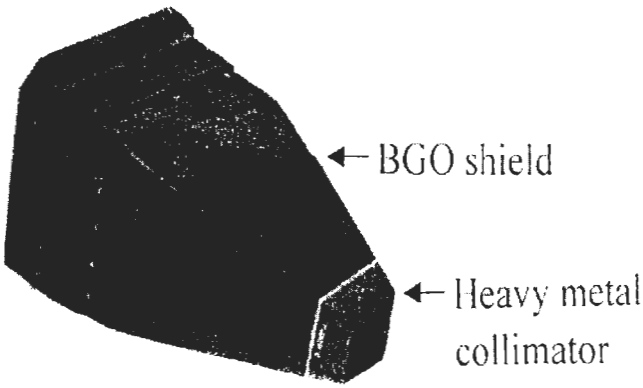

Figure 2.7: *A BGO Compton suppression shield specifically designed to house a standard Clover detector [Mab03].*

The Compton suppression factor (CSF) [Eml86, Sha88], or the background reduction, is obtained by taking the ratio of the unsuppressed to the suppressed spectrum. For the energy range of 300 - 800 keV, the CSF is obtained to be about 1.4 (illustrated in figure 2.8(b)).

The peak-to-total (P/T) ratio, a measure of the fraction of the total events in the crystal that have deposited their full photo-peak energy, is defined as the number of counts in the photo-peak (N_{peak}) to the total number of counts recorded in a spectrum (N_{total}), that is

$$P/T = N_{peak} / N_{total} \qquad (2.6)$$

A standard involving the measurement of the peak-to-total ratio for ^{60}Co source with photo peak energies at 1173 keV and 1332 keV has been set. This is depicted in figure 2.8 for both suppressed and unsuppressed spectra.

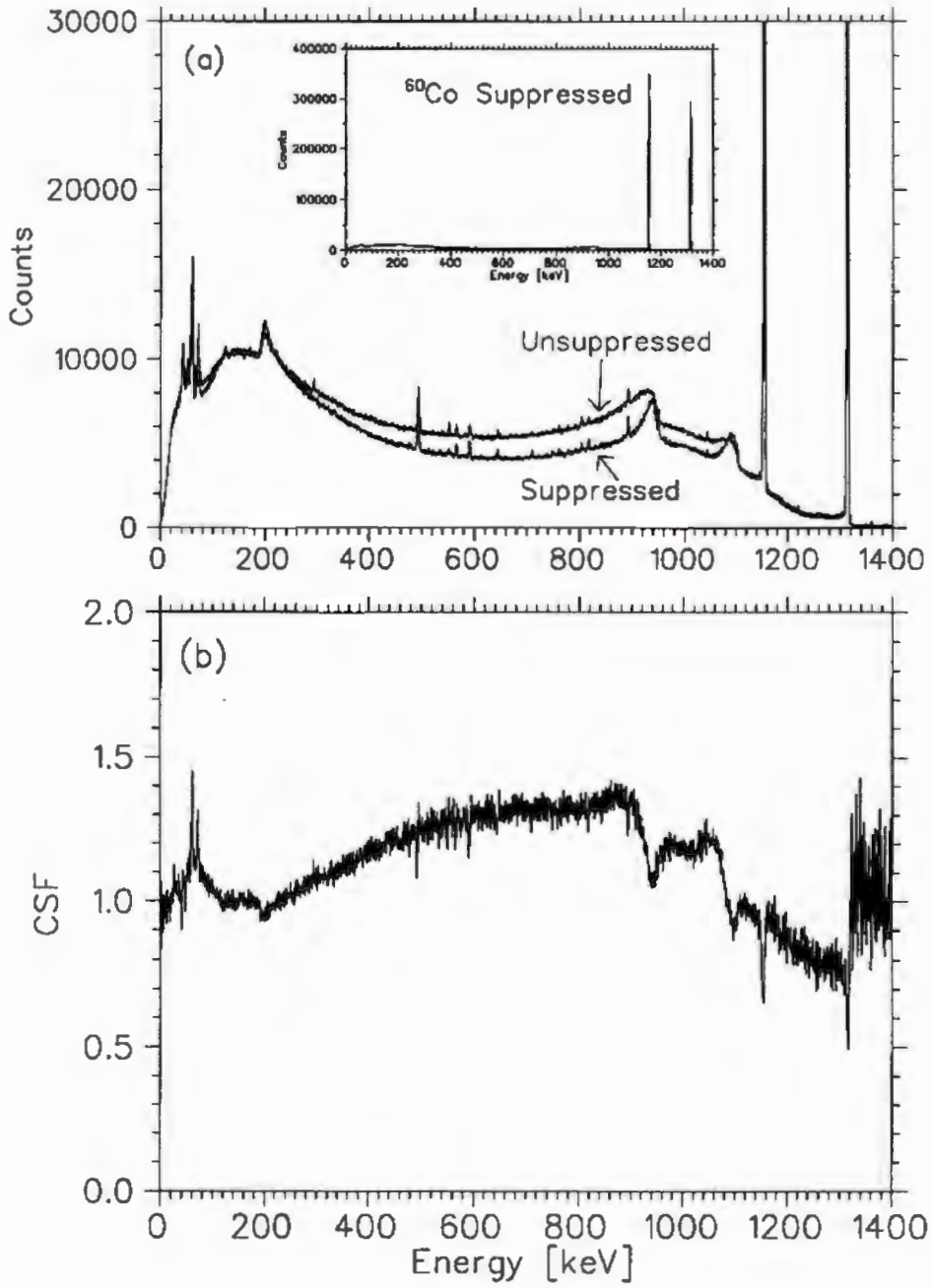

Figure 2.8: *(a) Compton suppressed and unsuppressed γ-spectra from a ^{60}Co radioactive source. (b) Compton-suppression factor (CSF) found from the ratio of the unsuppressed to the suppressed spectra. The CSF was found to be about 1.4. [Mab03]*

2.2.6 Proton Beam

A non-polarized proton beam was used to bombard the ^{208}Pb target at 4 different incident energies; namely, 11.6 MeV, 11.9 MeV, 13.2 MeV and 14.8 MeV. The number of protons that were accelerated at each energy corresponded to integrated beam intensities: $I_{11.6\ MeV}$ = 1.78 mAs, $I_{11.9\ MeV}$ = 2.96 mAs, $I_{13.2\ MeV}$ = 2.61 mAs and $I_{14.8\ MeV}$ = 2.49 mAs, respectively. Because of the singly positive charge nature of the proton beam, the intensity was measured in terms of the amount of charge recorded in a given time, that is, the electric current.

The proton beam was accelerated from the source through the low energy injection beam line, to the second solid pole injector cyclotron (SPC2), where it was pre accelerated to between 1/20 to 1/15 of its final energy as depicted in figure 2.4. Magnetic quadrupoles and solenoid lenses were used to focus the beam, whereas the dipole magnets were used to direct the beam to the AFRODITE target. Using dipole and quadrupole magnets, the beam was steered along the beam lines from the SPC2 and injected into the Separated Sector Cyclotron (SSC), where it was accelerated to its required energy.

Using high-energy beam lines, the beam was steered from the SSC and delivered to the F-line target chamber as shown in figure 2.4. The dipole and quadrupole magnets redirected and focused the beam to the lead target positioned in the center of the AFRODITE chamber. To minimize contamination during data collection, energy selective slits were inserted after the last 90^0 bending in the beam line, thereby reducing any particles surrounding the focal point at the target, called halo. This also minimized the broadening of the beam and avoided the beam hitting the target frame.

2.2.7 Target

The target used for this experiment was a 1 mg/cm^2 thick ^{208}Pb foil mounted on a target ladder inside the target chamber. The thin target was selected in order to ensure excellent resolution of the γ-rays and to avoid Doppler broadening of the peaks. The ladder has four different positions that can be used to mount the targets.

The target material (^{208}Pb), the aluminium oxide viewer (ruby) and an empty frame were loaded at different positions on the target ladder. The target ladder mounted on the hydraulic positioner was controlled from the data room with an automatic switch to allow the beam to be tuned. The beam was aligned by directing it through the hole in the center of

the ruby. When the beam interacts with ruby material, a bright light was observed on the monitor screen via the camera mounted on the target chamber. Using dipole magnets, quadrupole magnets and solenoid lenses, the beam was focused such that it passed through the center of the ruby. This occurred when the bright light initially observed, disappeared. To reduce halo, an empty target frame was positioned in the beam spot. After halo reduction, the ruby was put back again to check whether the beam was still aligned. Finally, the target ^{208}Pb was placed in the beam spot and data acquisition commenced.

2.2.8 Electronics and Data Acquisition Systems

Data acquisition used for this experiment at iThemba LABS was based on the MIDAS software package [MIDAS]. The MIDAS software was employed before (to adjust zero offsets, ADC thresholds and setting status words) and during the experiment to monitor on-line spectra, event rates and data acquisition in general.

The Nuclear Instrumentation Module (NIM) and Computer Automated Measurement and Control (CAMAC) electronic units were connected according to the circuit diagram depicted in figure 2.9. The circuit diagram shown in figure 3 is made up of two sub-circuits; (i) a timing circuit which is used to time-correlate the detected gamma rays and (ii) an energy circuit which gives us the information about the energy of the detected gamma rays. This energy information will then be used in the construction of the γ-γ matrix. Events containing both timing and energy information are written on the Digital Linear Tapes (DLT). Table 2.2 gives the details of the entire circuit [Rou01].

In order to obtain the required energy range, the detectors had to be operated in the positive polarity output because of the germanium detector preamplifier cut-off of about 1 V in negative polarity mode. This necessitated the changing of the 32 detector preamplifiers as well as the pulse processing electronics. About 15.5 8-hour shifts corresponding to useful beam on target were obtained for this experiment.

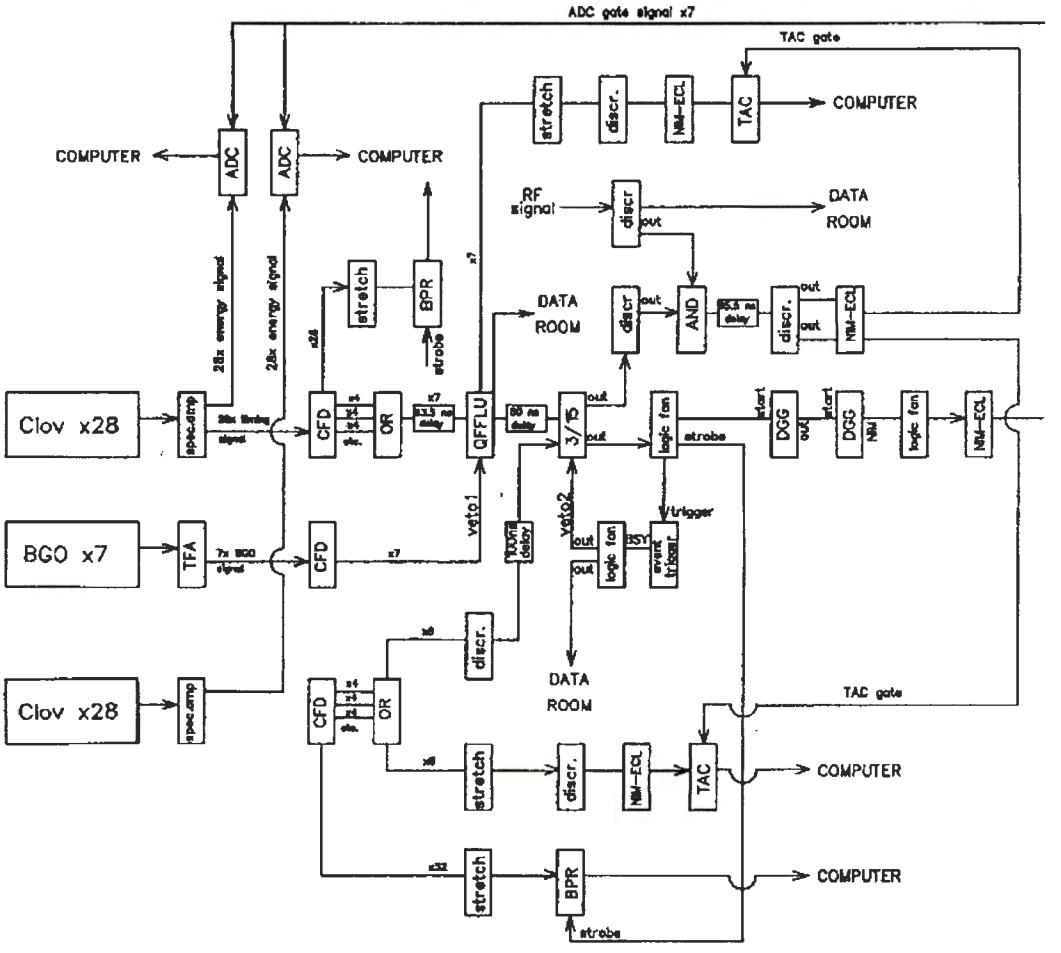

Figure 2.9: *The AFRODITE array electronics*

Module	Model
Analogue-to Digital-Converter(ADC)	Silena 4418/V
Bit Pattern Register (BPR)	iThemba LABS
Coincidence Unit	iThemba LABS
Constant Fraction Discriminator (CFD)	CAEN N415 or Ortec 934
Discriminator	Phillips 711 or LeCroy 821
Dual Gate Generator (DGG)	LeCroy 222
Event Trigger	iThemba LABS
Logic Fan-In/Fan-Out (FIFO)	LeCroy 429
NIM-ECL converter	EDA54 (iThemba LABS)
Quad Four-Fold Logic Unit (QFFLU)	Phillips 755
Spectroscopy Amplifier	CAEN N568
Stretcher	iThemba LABS
Time Amplitude Converter (TAC)	Silena 4418/T
Timing Filter Amplifier (TFA)	Ortec 474

Table 2.2: *Electronic modules used in an AFRODITE array*

Chapter 3

Data reduction and analysis procedure

The processes followed during the data analysis are indicated in the flow chart outlined in figure 3.1.

The coincidence data acquired during the $^{208}Pb(p,n\gamma)^{208}Bi$ and $^{208}Pb(p,2n\gamma)^{207}Bi$ experiments were stored as raw pulse heights onto the magnetic Digital Linear Tapes (DLT). After data acquisition, the event data were transformed into suitable form to facilitate the analysis procedure.

3.1 The experiment

This work is based on the study of the effect of the incident proton energy on the intensity of known gamma rays from the $^{208}Pb(p,n)^{208}Bi$ and $^{208}Pb(p,2n)^{207}Bi$ reactions. The γ-ray energies measured with the Clover detectors were rearranged into a matrix, a 2-D array of γ-ray energies that are in coincidence. Spectra were projected from the matrix using Radware software, notably the GF3 ("gelifit") program, which was used to view the spectra. The total projection spectra (see section 3.6) of the matrices at four different proton energies are shown in figure 3.2 to figure 3.5. From the Table of Isotopes [Fir96], γ-ray transitions belonging to ^{208}Bi and ^{207}Bi were identified.

3.2 Data Analysis

The Clover detectors are used to measure the γ energies associated with the reaction products which are then arranged into a two-dimensional array of coincident γ-energies that is commonly termed a matrix.

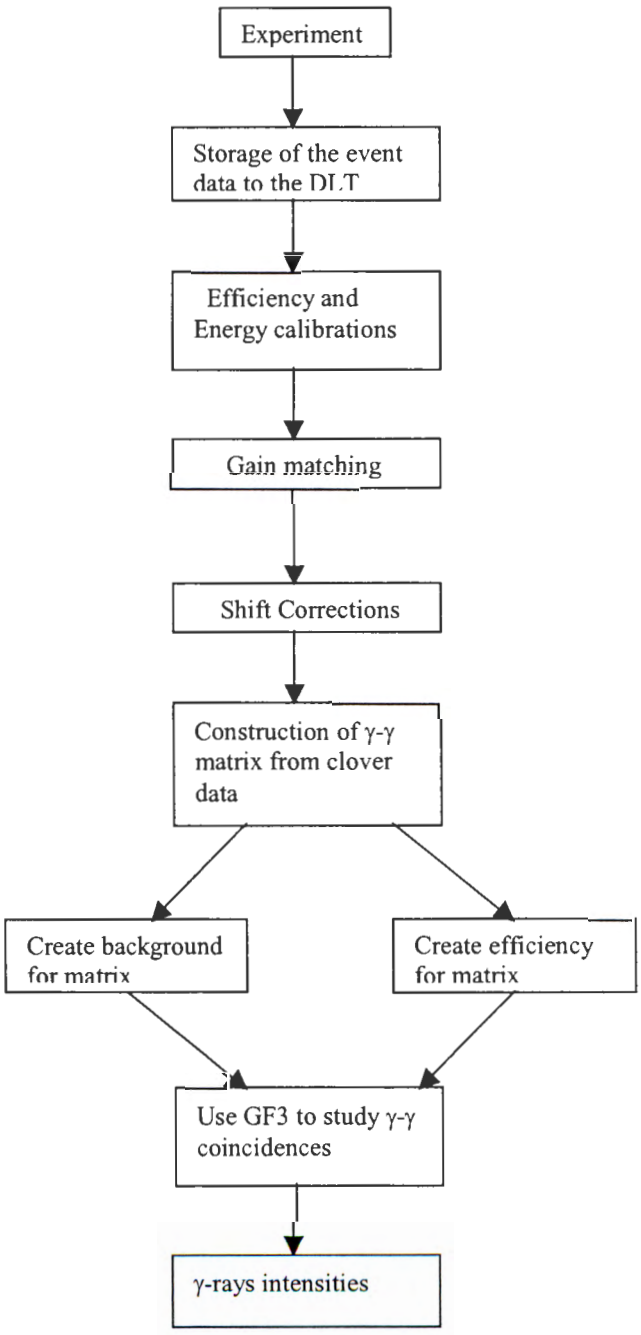

Figure 3.1: *Schematic step-by-step representation of the processes followed during the data analysis.*

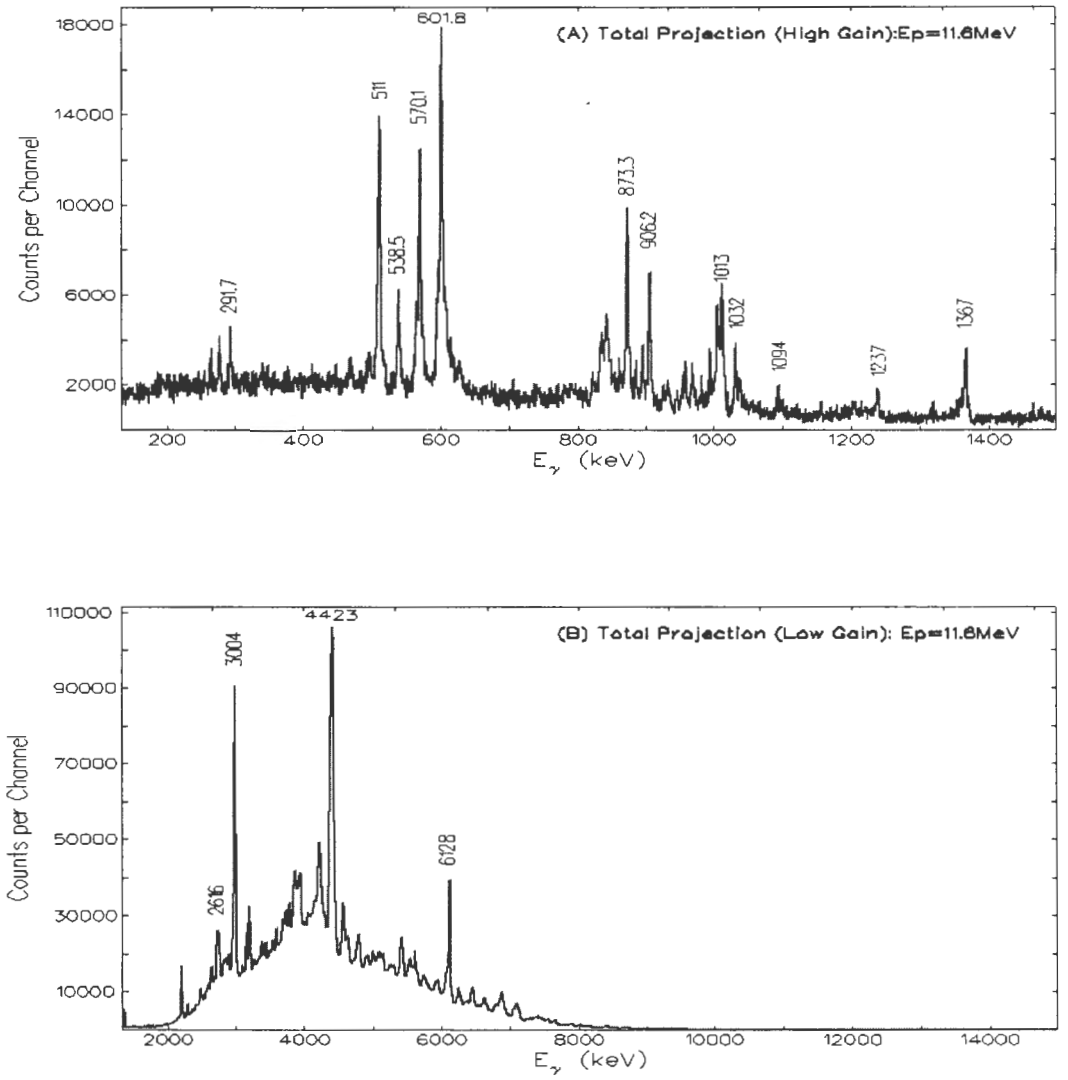

Figure 3.2: *(A) Total projection of the high gain matrix for the energy range 0 < E_γ < 1500 keV at beam energy of 11.6 MeV.*
(B) Total projection of the low gain matrix for the energy range 1000 keV < E_γ < 15000 keV at beam energy of 11.6 MeV.

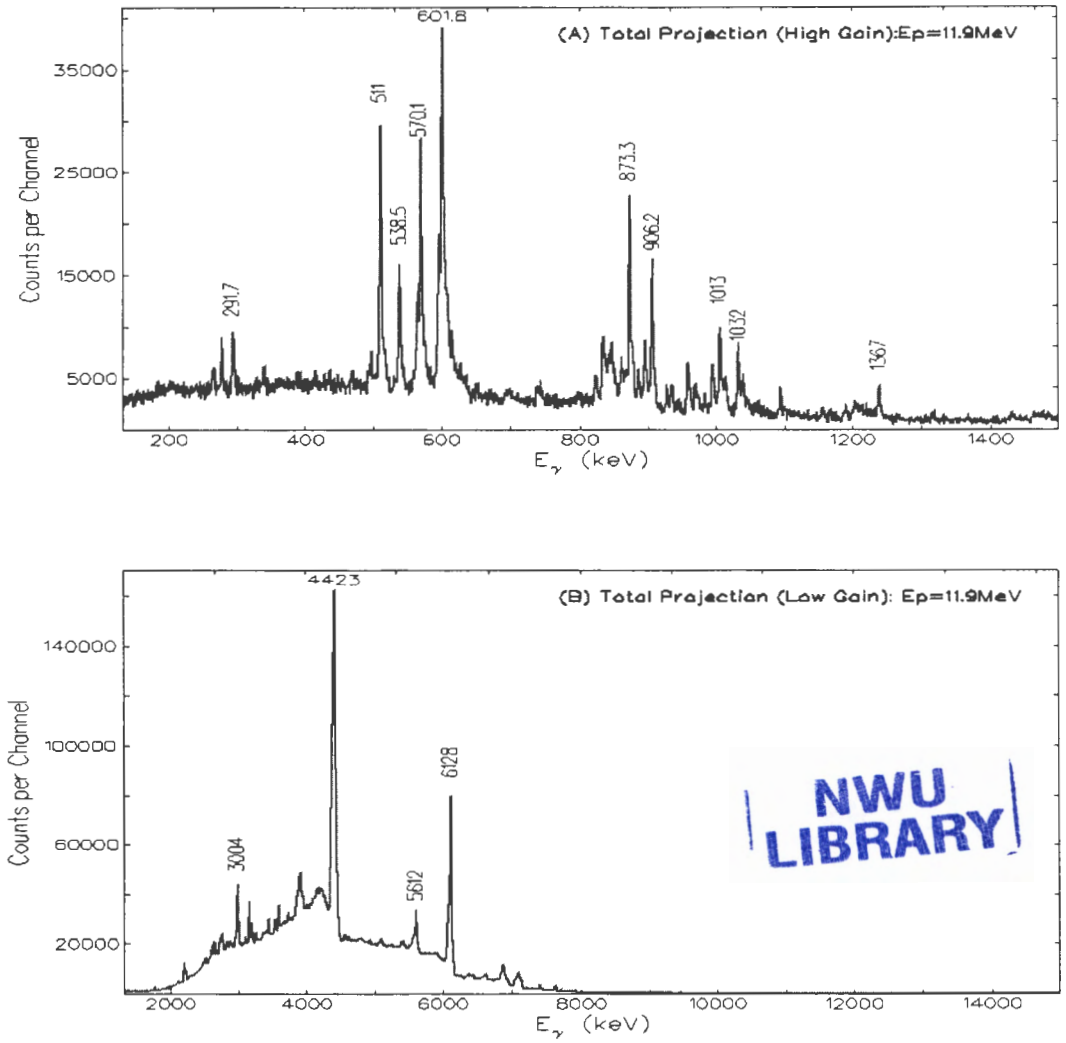

Figure 3.3: *(A) Total projection of the high gain matrix for the energy range* $0 < E_\gamma < 1500$ *keV at beam energy of 11.9 MeV.*

(B) Total projection of the low gain matrix for the energy range $1000\,keV < E_\gamma < 15000$ *keV at beam energy of 11.9 MeV.*

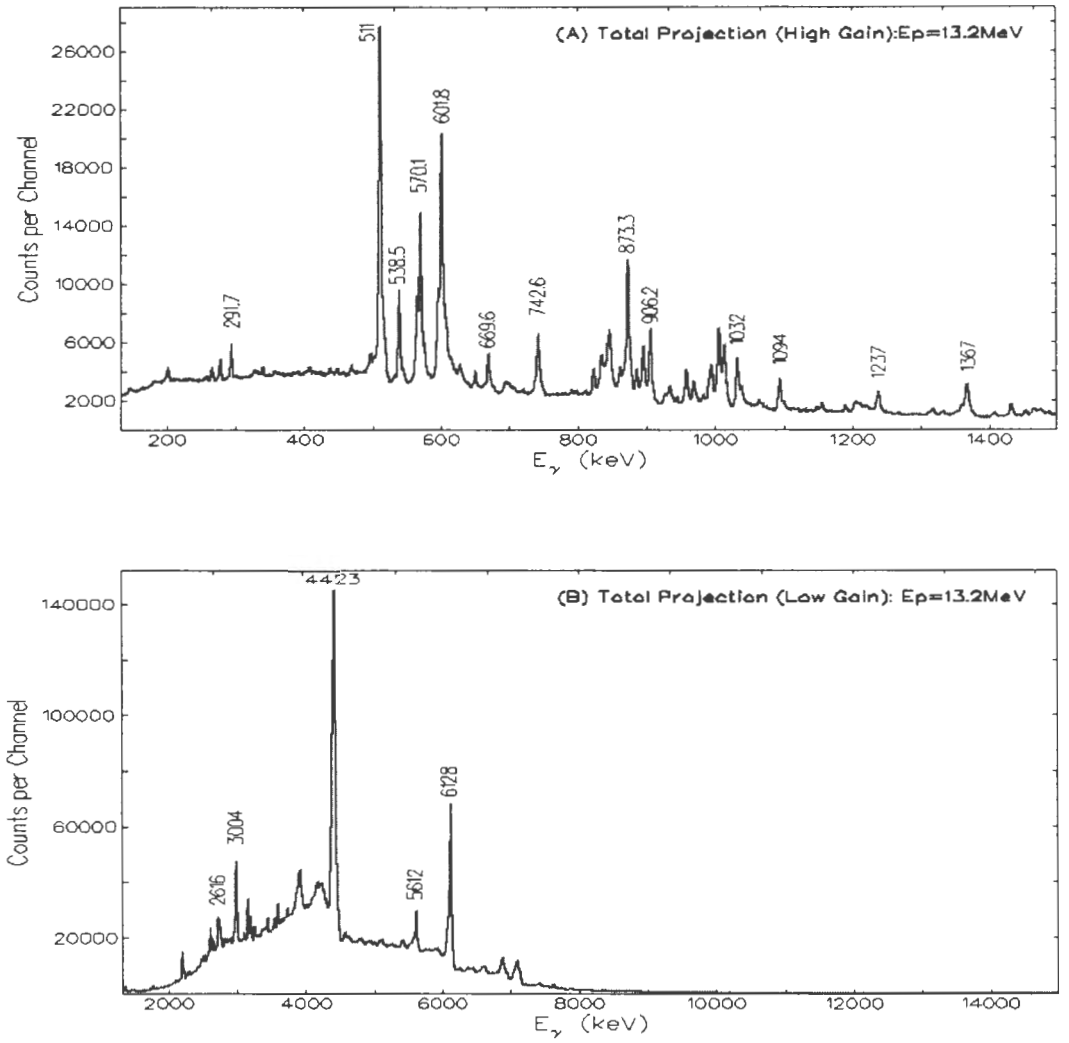

Figure 3.4: *(A) Total projection of the high gain matrix for the energy range $0 < E_\gamma < 1500$ keV at beam energy of 13.2 MeV.*
(B) Total projection of the low gain matrix for the energy range 1000keV $< E_\gamma$ < 15000 keV at beam energy of 13.2 MeV.

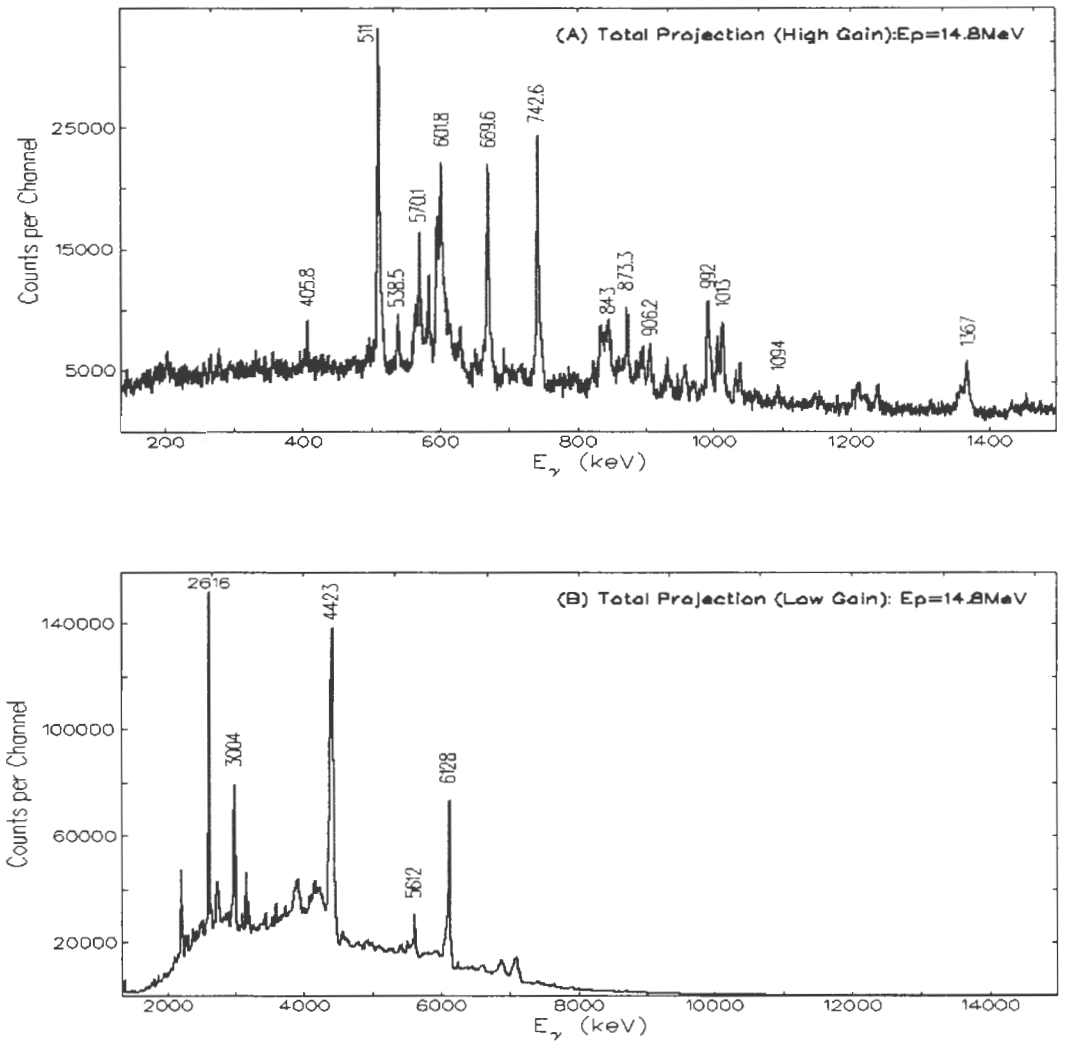

Figure 3.5: *(A) Total projection of the high gain matrix for the energy range $0 < E_\gamma < 1500$ keV at beam energy of 14.8 MeV.*
(B) Total projection of the low gain matrix for the energy range $1000keV < E_\gamma < 15000$ keV at beam energy of 14.8 MeV.

Programs from RADWARE were used to project and view coincidence spectra from the matrix. RADWARE is a collection of γ-ray analysis programs developed by David Radford [Rad00]. The main ones employed in the analysis of data in this work include:

- SLICE – used to generate background-subtracted, gated spectra and total projections from the matrix
- GF3 ("gelifit") – a graphical spectrum display and analysis program used to set the window regions for the SLICE program to generate 1-D gates. It is also used to perform peak fitting.

3.3 Energy and Efficiency calibrations

At the end of the experiment, energy and efficiency calibration measurements were performed for the Clover detectors. This was done to facilitate the energy assignments to the pulse height channels. The energy calibration parameters required for use in the GF3-program were generated from the ^{60}Co, ^{40}K and ^{56}Co sources. The energy calibration was also checked using the known 511 keV and the 2614 keV ^{208}Pb lines. The calibration sources were placed inside the target chamber (figure 2.4) at the target position and data were collected for 30 minutes. The centroids of the photopeak from the source spectra were determined using the GF3 program, a peak-fitting program. There are different forms of fitting equations, from linear to quadratic etc. In the case where the fit is linear, as performed in this experiment, this program fits a linear function having the form $E_{ch} = Bm + A$, generating a set of linear energy calibrations parameters (LECP); namely m and A for all elements of the Clover detector used during the experiment. A is the offset. E_{ch} represents true γ-ray energy and B *(keV/ch or dispersion)* represents the digitized pulse height. The value of the dispersion, B is obtained from the relation:

$$B = \frac{E_2 - E_1(keV)}{ch_2 - ch_1} \tag{3.1}$$

where ch_1 is the channel corresponding to the peak energy E_1, and ch_2 is the channel corresponding to the peak energy E_2.

The efficiency calibration parameters for the Clovers were determined with the ^{152}Eu and ^{133}Ba source data by [Mab03]. From the efficiency curve for the 8 Clovers outlined in figure 3.6, the maximum detection efficiency of the Clover detectors occurred at 110keV, mainly due to the absorption and CFD thresholds, and decreased smoothly with increasing energy. This characteristic behavior responsible for the rise and then the decrease in efficiency of the detectors is due to:

(a) The decrease in photoelectric effect with increasing γ-ray energy; and

(b) The decrease in the Compton scattering cross-section with increasing γ-ray energy.

The calculated energy and efficiency parameters were then provided to the GF3-program to be used during the search of the γ-γ coincidence relationships.

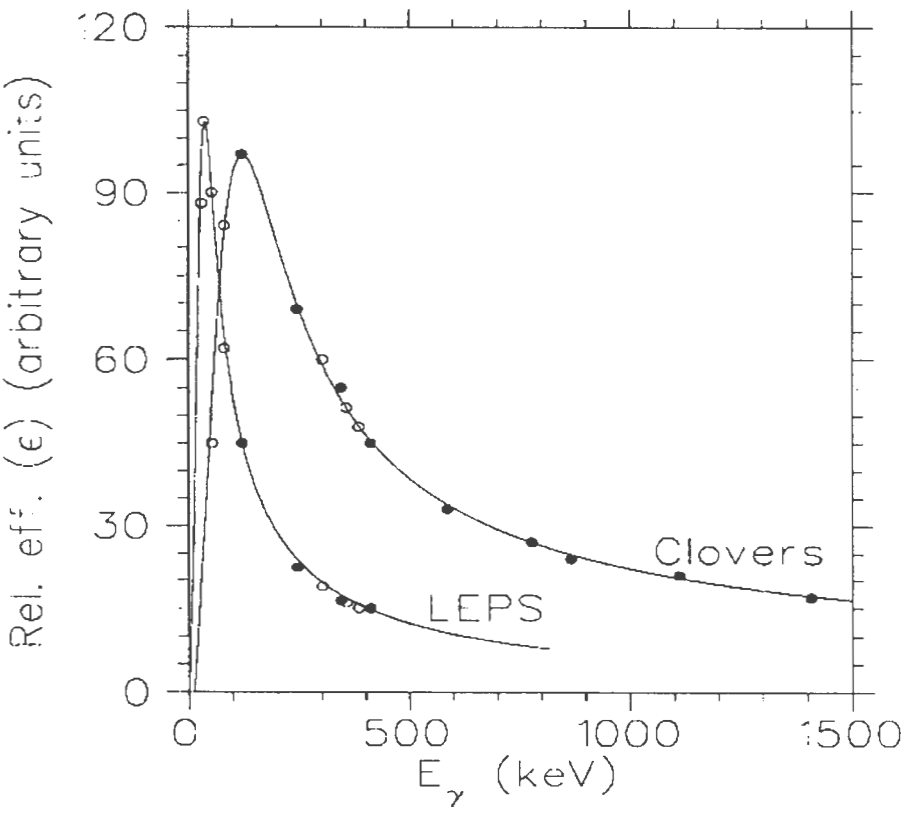

Figure 3.6: *The relative efficiency for the 7 Clover and 8 LEPS detectors measured with ^{152}Eu (filled-circles) and ^{133}Ba (open circles) radioactive sources placed on the target ladder at the target position [Mab02].*

3.4 Gain matching

The in-beam data stored on the magnetic DLT were sorted in order to trace possible detector gain-drifts that might have occurred. Investigations into the cause of such gain-drifts have been conducted by Dowie and Mullins [Dow00]. From their investigations, there is a possibility that the temperature fluctuations in the AFRODITE vault may have an effect on the amplifiers such that drifts occur in the output signals. Therefore gain matching plays an important role in pre-data analysis procedure.

For gain matching, a correctly calibrated and positioned spectrum obtained from the first runs, the in-beam reference spectrum (IRS), was chosen as a reference. The in-beam reference spectrum (IRS) was chosen for each incident proton energy. The reference spectrum and other spectra were collected in a GF3.CMD file so that they can be compared using the GF3 program. Gain matching was done by comparing and following the movement of the strongest peaks in the data. The reference peaks used in the drift corrections were 511 keV, 1360 keV, the aluminum doublet at 3004 keV, the 2614 keV line and the 6128 keV ^{16}O and its escape peak. These peaks are shown in figures 3.2-3.5. Therefore, to match to say 1 keV/channel, calibration parameters can be used as gain corrections. Then for 0.5 keV/channel, then gain correction will be:

Gain correction = 2 x calibration parameter.

The gain correction factor for this experiment was chosen to be 1.5 ≡ 0.6 keV/ch

3.5 Doppler Shift Corrections

The Doppler-shift corrections for the γ-rays detected were necessitated by the use of a thin ^{208}Pb target as described in sections 2.2.6 and 2.2.7. The recoiling residual nucleus emits γ-rays subjected to energy shifts according to the equation:

$$E_\gamma = E^0_\gamma(1 + \beta\cos\theta) \qquad (3.2)$$

where $\beta = v/c$ (v is the recoil velocity of the nucleus and c is the speed of light), E_γ is the Doppler shifted γ-ray energy, E^0_γ is the unshifted γ-ray energy (detected normal to the recoil nucleus velocity axis) and θ is the angle between the detector and the

recoil beam axis. Comparing the recoil velocity of the large nucleus (^{207,208}Bi) and that of light, the value of $\beta = v/c$ was considered to be negligibly small. According to equation 3.2, maximum Doppler shift occurs at $\theta = 0^0$ and the minimum Doppler shift is at $\theta = 0^0$ since the $\cos 90^0 = 0$.

The energy difference between the energy entering the detector at angle $\theta + d\theta$ and the one entering at an angle $\theta - d\theta$ is given by:

$$\Delta E = \left| E_\gamma(\theta + d\theta) - E_\gamma(\theta - d\theta) \right| \tag{3.3}$$

then

$$\Delta E = 2\, E^0_\gamma \sin\theta \sin d\theta \tag{3.4}$$

From equation 3.4, the Doppler effect broadening is maximum at $\theta = 90^0$ and zero at $\theta = 0^0$. Therefore to improve the energy resolution near $\theta = 90^0$, the solid angle of the detector must be reduced.

3.6 E_γ-E_γ Matrices

The gamma-gamma matrix is a 2-dimensional ($E_{\gamma 1}$,$E_{\gamma 2}$) energy histogram with the energy of one photon on one axis and the energy of a coincident photon on the other axis. The total projection of the matrix is formed by the projection of all the counts onto one energy axis, resulting in one-dimensional γ-ray spectrum. Setting a gate on a particular photo- peak using channel numbers from the total projection spectrum generates a coincidence spectrum of all gamma rays associated with that photo peak. This spectrum will also contain events, which are in coincidence with the Compton background on which the photo peak sits. The background spectrum, consisting of random coincidences and unsuppressed Compton events from the discrete and continuum γ-rays, is subtracted from the gated spectrum, producing a coincidence spectrum for a particular γ-ray photo peak observed in the total projection. This was achieved by using a BG command in the GF3 program (or alternatively the Set Count (SC) command to write a background spectrum manually, thereby cutting off the peaks in the spectrum), thus creating a background spectrum, which will then be

subtracted from the gated matrix. The resulting γ-spectra are plotted in section 4.1 (figure 4.2– 4.6) for ^{208}Bi and section 4.3 (figure 4.9 – 4.12) for ^{207}Bi. Only the "high gain" gamma-gamma matrices were considered, since most of the γ-ray transitions belonging to ^{207}Bi and ^{208}Bi lie in the energy range below 2.0 MeV.

3.7 Transition Intensities

The 'relative' amount of the products, in this case ^{207}Bi and ^{208}Bi as a function of proton energy, without considering the integrated beam, I_γ, is given by

$$I_\gamma = S / \epsilon \tag{3.5}$$

where S represents the area of the γ-ray transition or the number of counts in a particular peak and ϵ the detector efficiency for the γ-ray obtained in section 3.3.
The 'absolute' amount of the products at different proton energies I, is given by:

$$I = I_\gamma / I_E \tag{3.6}$$

Where I_E is the integrated beam - the amount of beam that hit the target during the run at different proton energies. The I_E values at four proton energies are given in section 2.2.6.

Chapter 4

Results of Data Analysis

This chapter presents the experimental results based on the γ-γ coincidence relationships and transition intensities for the ^{207,208}Bi nuclei. Interpretation of the experimental results in relation to the predicted compound nucleus formation model, its γ-decay and the subsequent evaporation of neutrons as the beam energy is increased are presented. A consistent relationship between the beam energy and the intensity of the residual ^{207,208}Bi nuclei is established.

4.1 ^{208}Bi γ-γ coincidences

From the spectra obtained, the five most intense ^{208}Bi peaks were chosen for analysis at each proton energy as discussed in section 3.6 above. The peaks are 538.5 keV, 570.1 keV, 601.8 keV, 873.3 keV and 906.2 keV. From the γ-ray coincidence spectra, γ-ray transitions due to the ^{208}Pb(p,n)^{208}Bi reaction are observed. The resulting γ-ray coincidence spectra representing single gates set on 538.5 keV, 570.1 keV, 601.8 keV, 873.3 keV and 906.2 keV transitions are plotted in figures 4.2 – 4.6. Partial decay level scheme [Pro70] for the transitions discussed in this section (section 4.1, figures 4.2 – 4.6) is given in figure 4.1.

The 4^+ state at 601.5 keV level decays to the 4^+ state at 63.3 keV via the 538.5 keV transition. Setting 538.5 keV gates in figures 4.2 (A-D) exhibit coincidence relationships with the weak 291.7 keV and 906.2 keV transitions. The 601.8 keV transition is weakly observed in all four cases. This should not be the case.

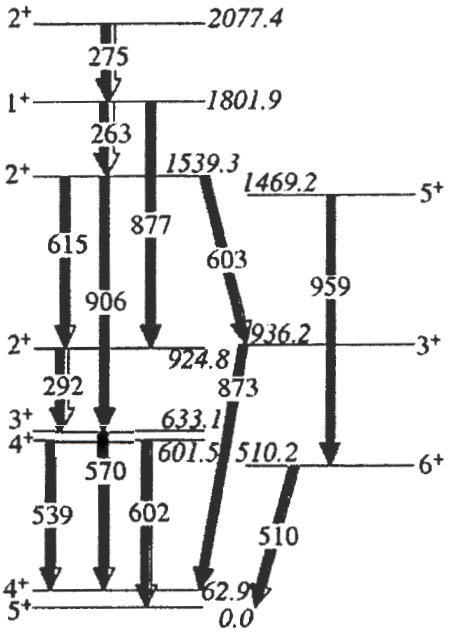

Figure 4.1: *Partial level decay scheme of ^{208}Bi from the transitions shown in figures 4.2 – 4.6 [Pro70].*

The 601.8 keV and 538.5 keV transitions should not be in coincidence since the 601.8 keV and the 538.5 keV decay from the same level. That is, the level decays either by the 601.8 keV or the 538.5 keV (figure 4.1). The appearance of the 601.8 keV is due to the 601.8 keV and 603.3 keV doublets, which are a mutually coincident pair.

The 570.1 keV gates in figures 4.3 (A-D) display coincidence relationships with the 906.2 keV and 994.8 keV transitions. The 3^+state at 633.1 keV level decays to the 4^+ at 63.3 keV via the 570.1 keV .

There is a very strong transition to the ground state from the 601.8 keV level. Spectra produced by gating on the 601.8 keV transition shown in figures 4.4 (A-D) exhibit coincidence relationships with the 906.2 keV and 873.3 keV transitions.

Gating on the 873.3 keV transition results in the spectra shown in figures 4.1 and 4.5 (A-D) where coincidence relationships with the 603.3 keV transition are clearly seen. The 3^+state at 936 keV level makes a strong transition to the 4^+state at 63.3 keV.

The 2^+state at 1539.8 keV level decays to the 3^+state at 633.3 keV level. The 906.2 keV gates in figures 4.6 (A-D) exhibit coincidence relationships with the 262.7 keV, 275.4 keV, 538.5 keV, 570.1 keV and the 601.8 keV transitions. The 262.7 keV and 275.4 keV transitions are weakly observed.

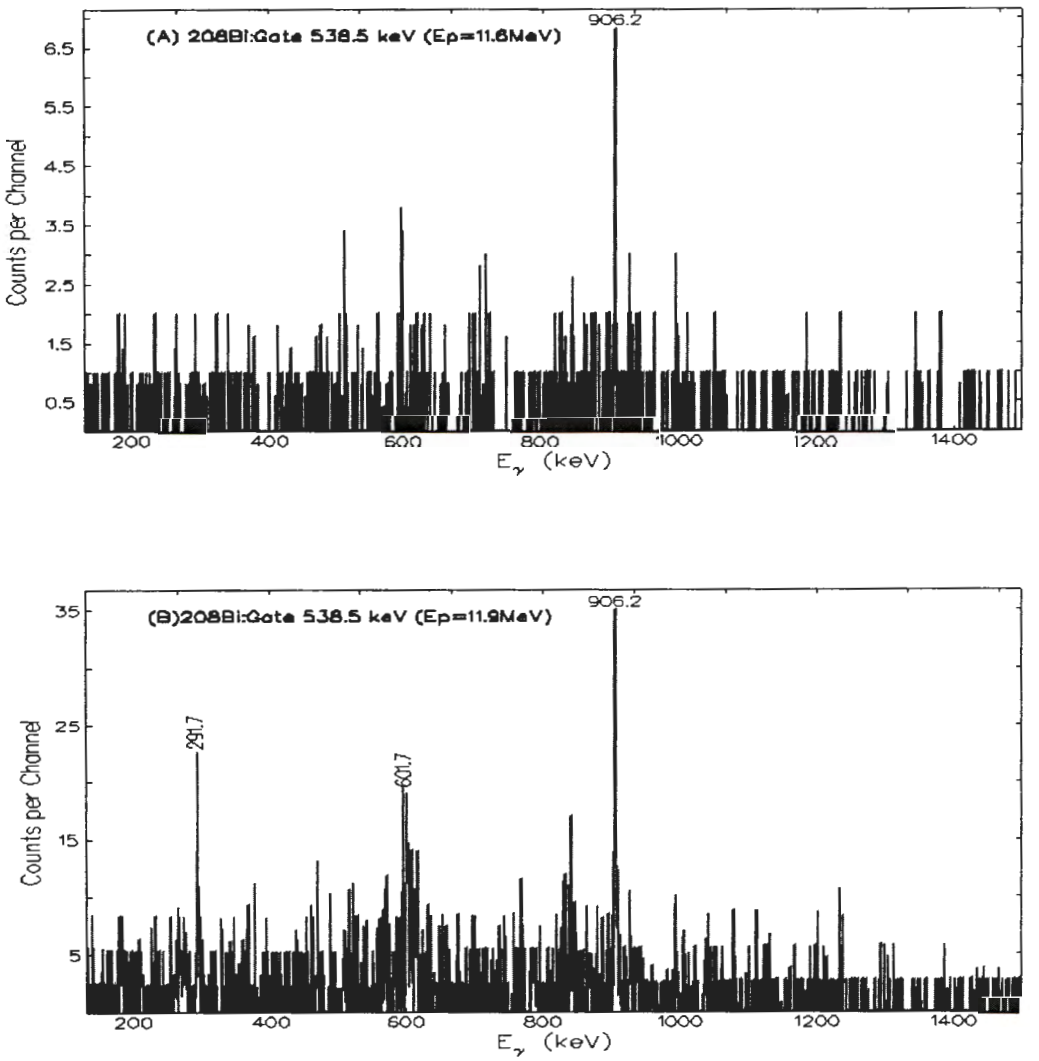

Figure 4.2 (A-B): *Coincidence γ-ray spectra gated on the 538.5 keV ^{208}Bi γ-ray transition for the 11.6 MeV (A) and 11.9 MeV (B) beam energy.*

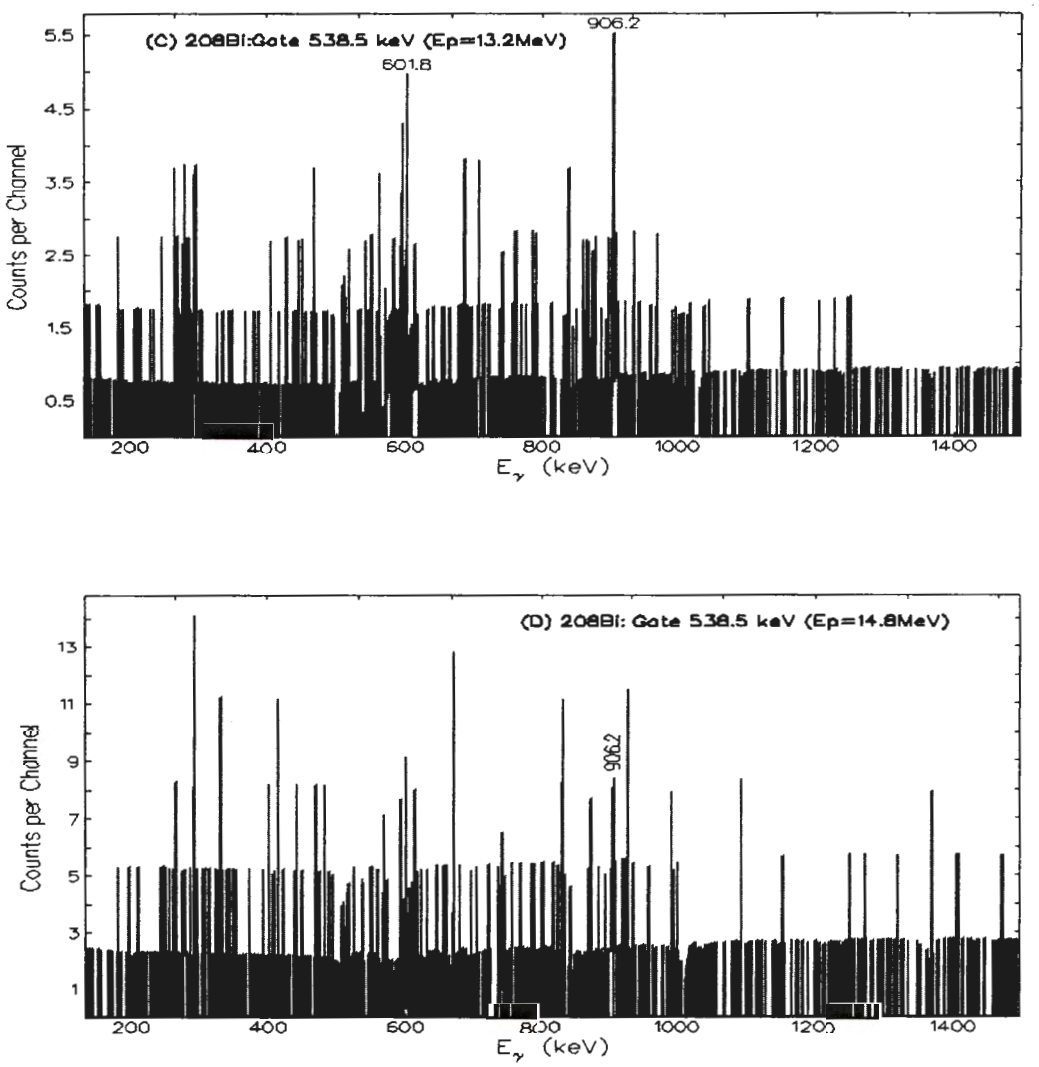

Figure 4.2 (C-D): *Coincidence γ-ray spectra gated on the 538.5 keV ^{208}Bi γ-ray transition for the 13.2 MeV (C) and 14.8 MeV (D) beam energy.*

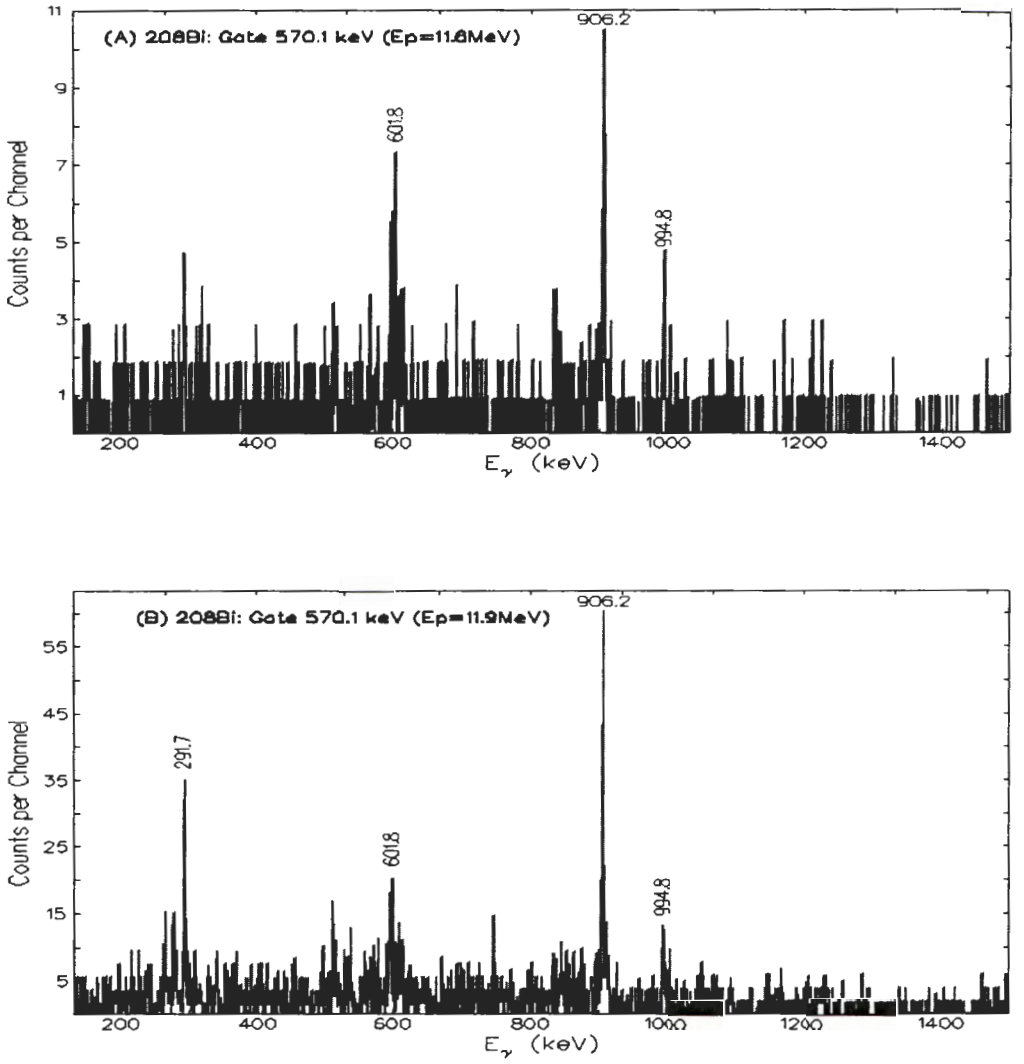

Figure 4.3 (A-B): *Coincidence γ-ray spectra gated on the 570.1 keV ^{208}Bi γ-ray transition for the 11.6 MeV (A) and 11.9 MeV (B) beam energy. The 601.8 keV transition should not be in coincidence with the 570.1 keV. This transition is mainly due to the existence of the 601.8 keV and 603.3 keV mutually coincidence pair as discussed in the text.*

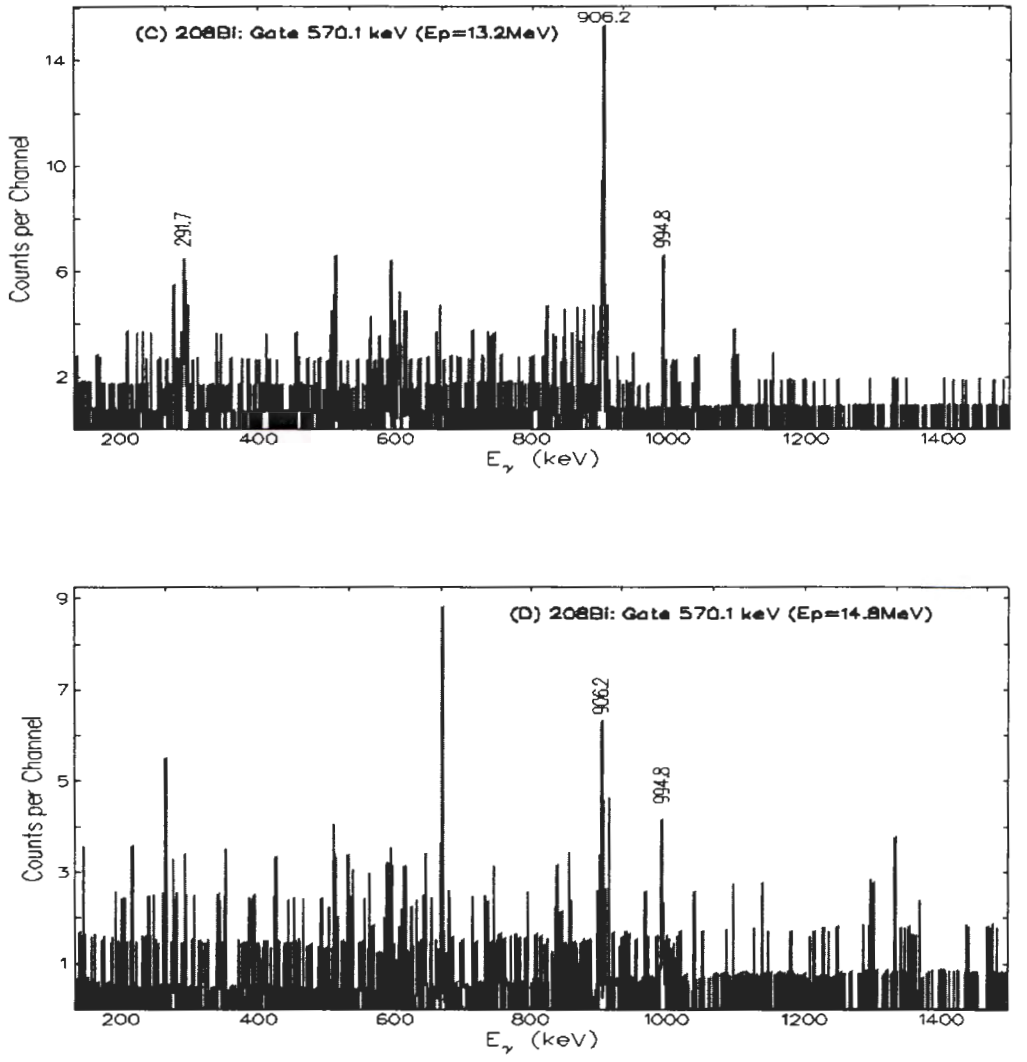

Figure 4.3 (continued) (C-D): *Coincidence γ-ray spectra gated on the 570.1 keV ^{208}Bi γ-ray transition for the 13.2 MeV (C) and 14.8 MeV (D) beam energy. The 601.8 keV transition in (C) should not be in coincidence with the 570.1 keV. This transition is mainly due to the existence of the 601.8 keV and 603.3 keV mutually coincidence pair discussed in the text.*

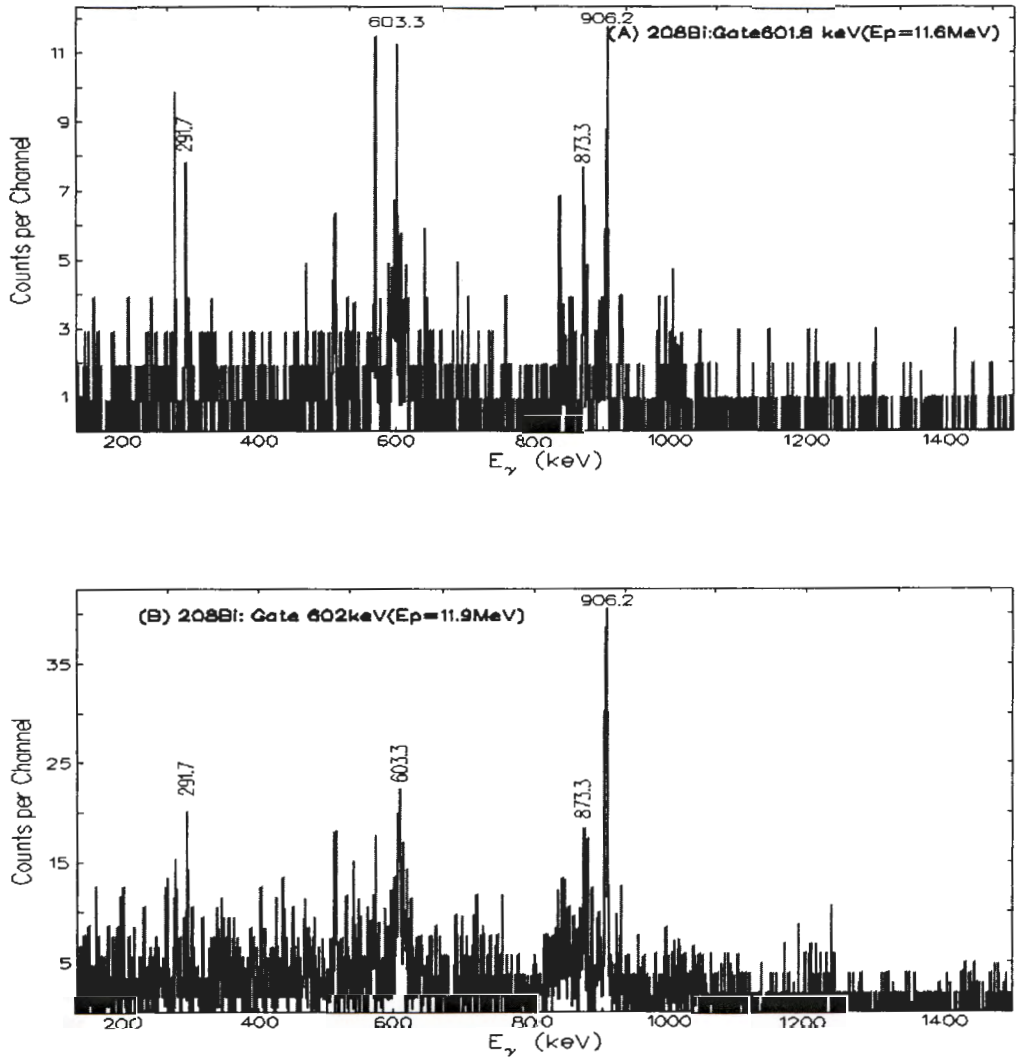

Figure 4.4(A-B): *Coincidence γ-ray spectra gated on the 601.8 keV ^{208}Bi γ-ray transition for the 11.6 MeV (A) and 11.9 MeV (B) beam energy. The presence of the 601.8 keV transition in both (A) and (B) is due to the 601.8 keV and 603.3 keV mutually coincidence pair.*

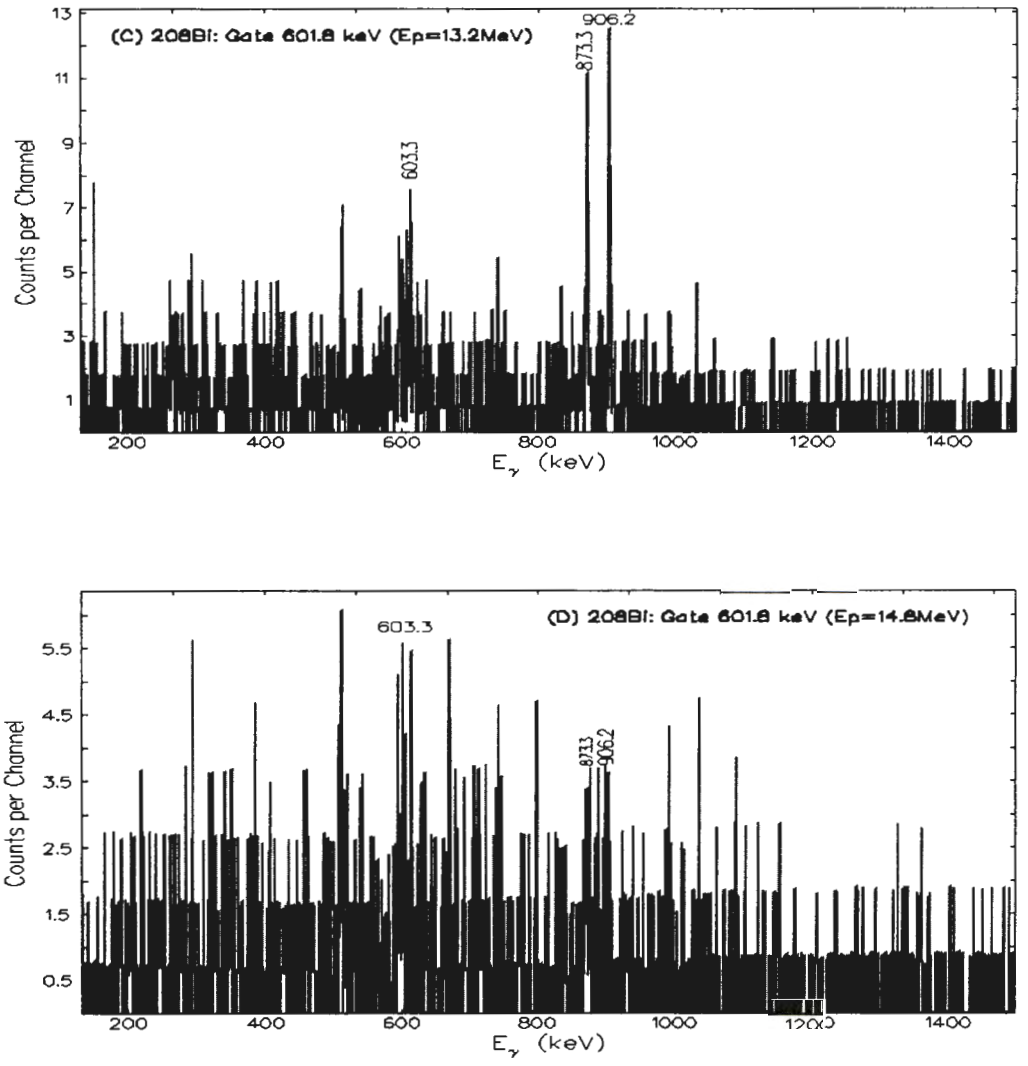

Figure 4.4 (continued) (C-D): *Coincidence γ-ray spectra gated on the 601.8 keV ^{208}Bi γ-ray transition for the 13.2 MeV (C) and 14.8 MeV (D) beam energy.*

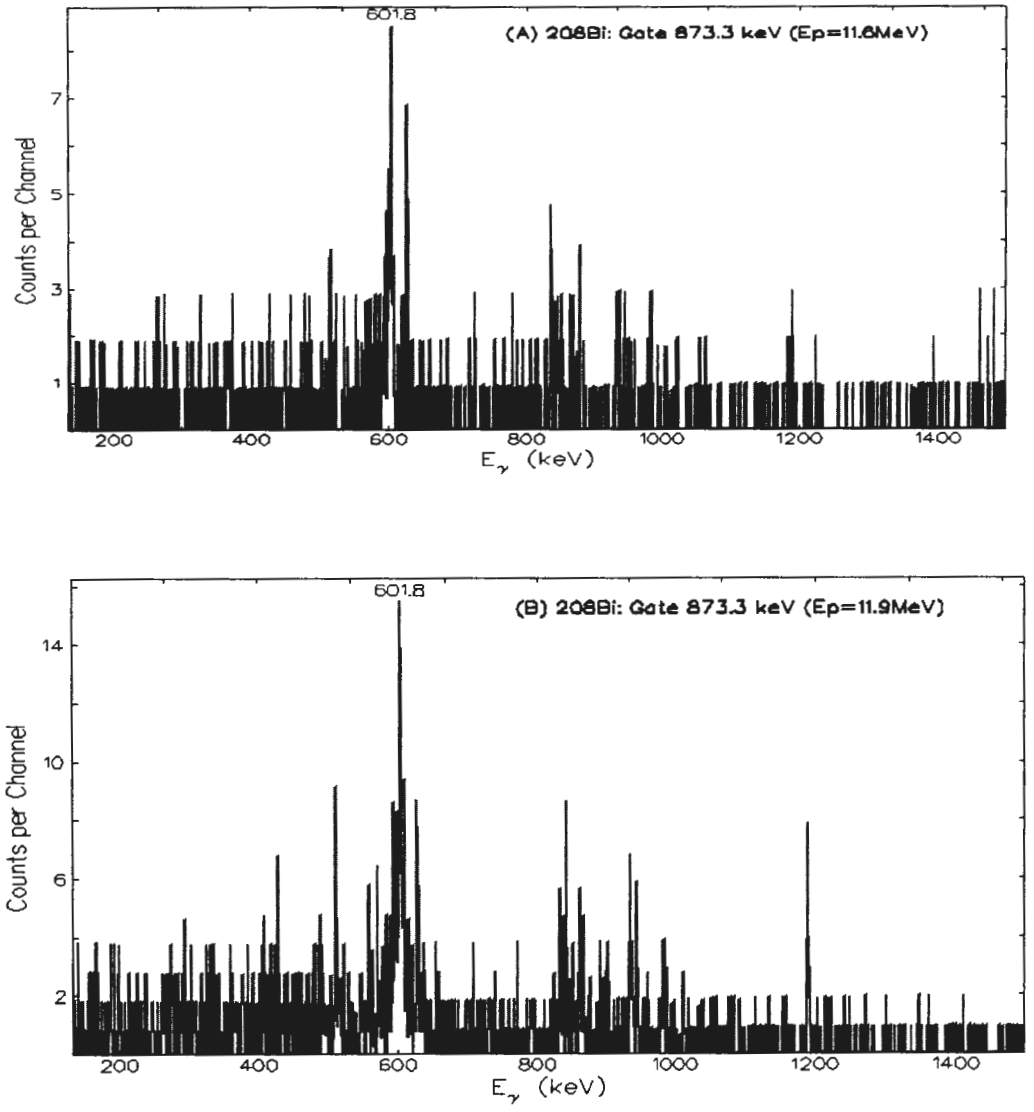

Figure 4.5 (A-B): *Coincidence γ-ray spectra gated on the 873.3 keV ^{208}Bi γ-ray transition for the 11.6 MeV (A) and 11.9 MeV (B) beam energy.*

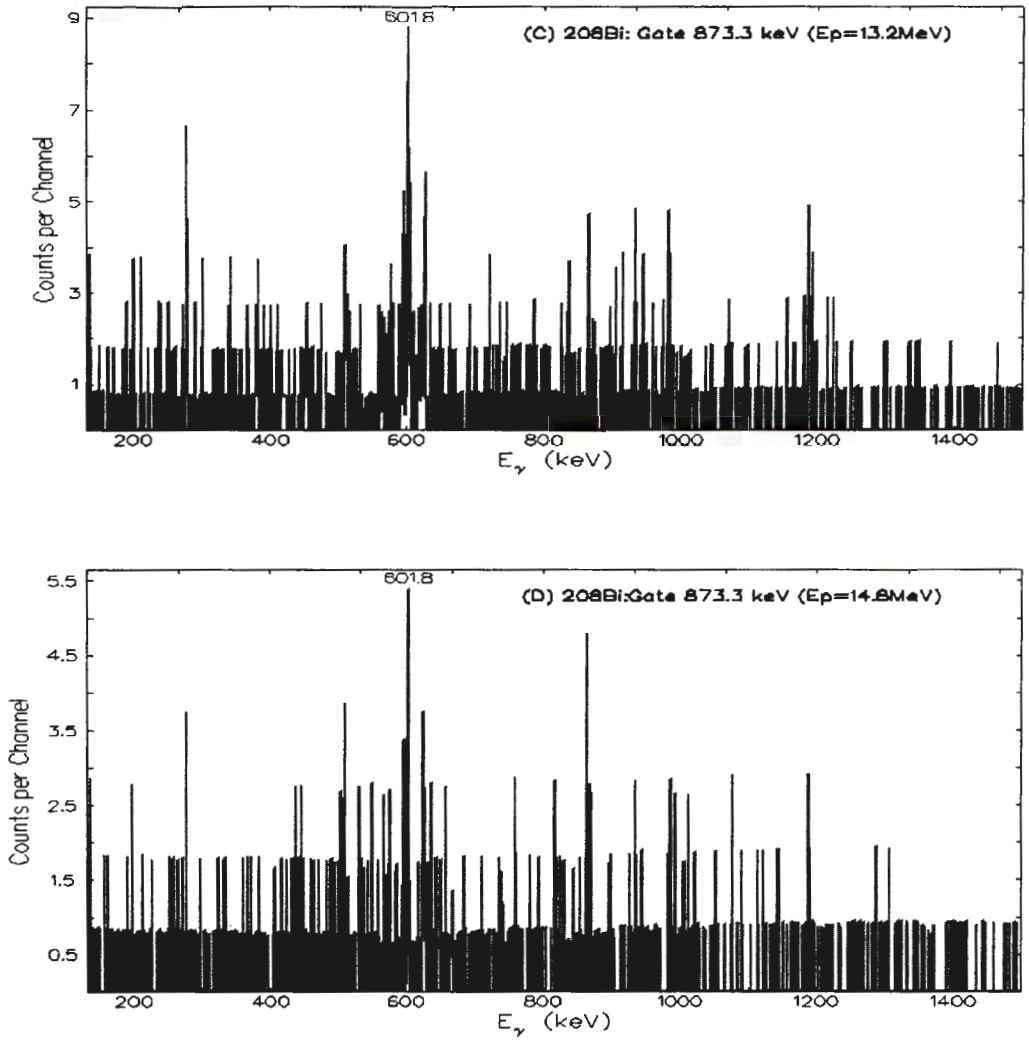

Figure 4.5 (continued) (C-D): *Coincidence γ-ray spectra gated on the 873.3 keV ^{208}Bi γ-ray transition for the 13.2 MeV (C) and 14.8 MeV (D) beam energy.*

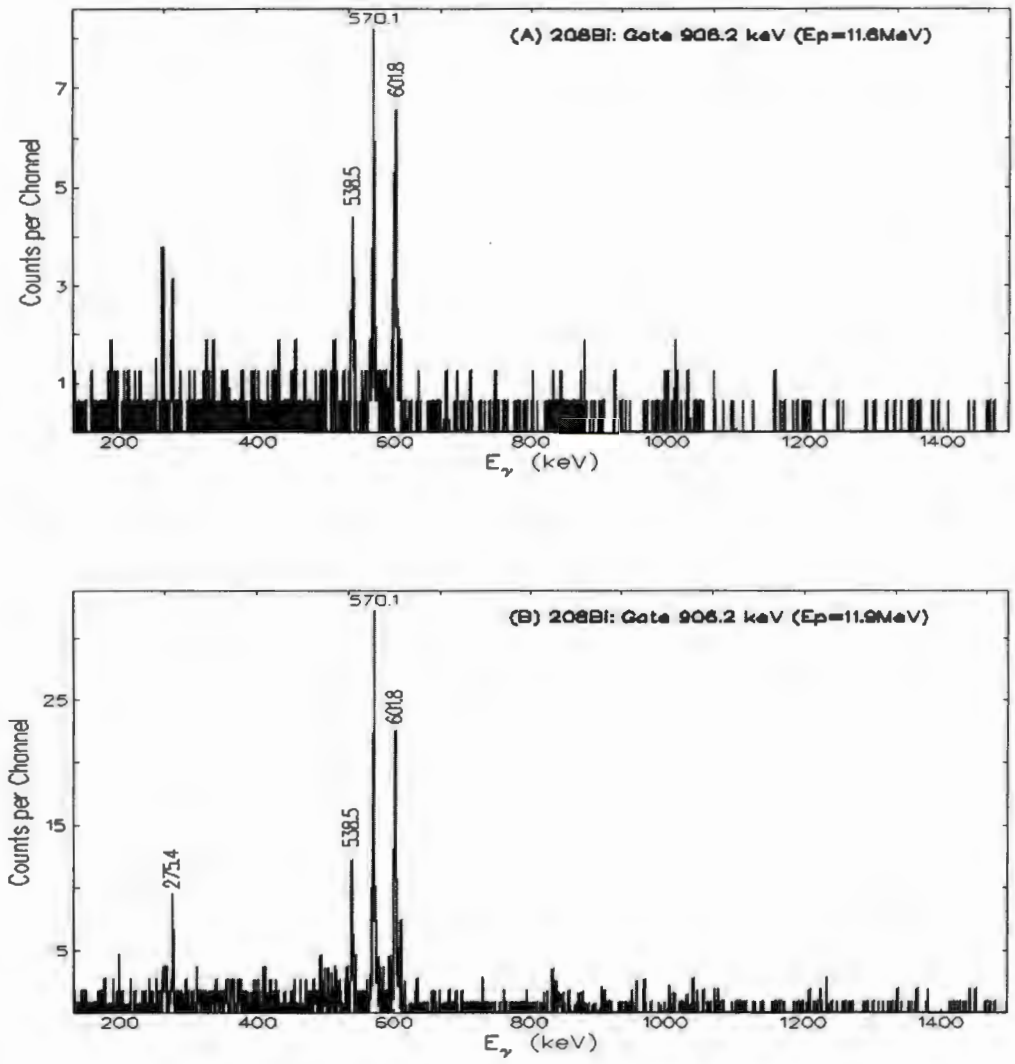

Figure 4.6 (A-B): *Coincidence γ-ray spectra gated on the 906.2 keV ^{208}Bi γ-ray transition for the 11.6 MeV (A) and 11.9 MeV (B) beam energy.*

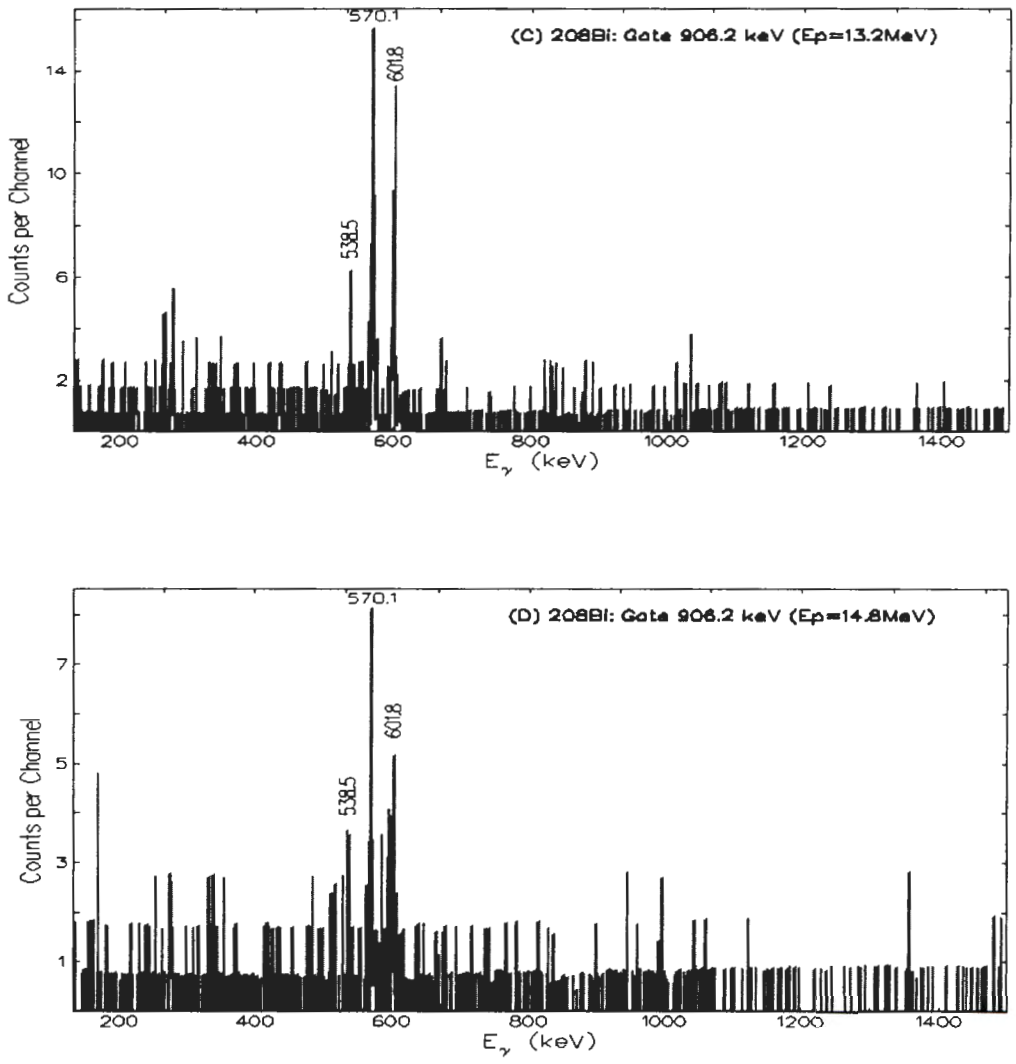

Figure 4.6 (continued) (C-D): *Coincidence γ-ray spectra gated on the 906.2 keV ^{208}Bi γ-ray transition for the (C) 13.2 MeV and (D) 14.8 MeV beam energy.*

4.2 Transition Intensities for ^{208}Bi

The relative (I_γ) and absolute (I) γ-ray intensities for the five transitions at four different beam energies were determined from the total projections by obtaining the areas of each identified peak using the GF3 program and employing equations 3.5 and 3.6 (Appendix 1A). The relative gamma intensities were determined when the peaks were corrected for the detector relative efficiency (assuming 5% uncertainty). The results are listed in table 4.1. The relationships between the absolute intensities (I) as functions of the beam energy for each γ-ray transition are illustrated in figures 4.7(a-e). The relative intensities normalised to the most intense peak, the 601.8 keV transition, are listed in table 4.2 (see appendix 1B).

E_γ (keV)	Absolute γ-ray intensity(I) (11.6 MeV)	Absolute γ-ray intensity(I) (11.9 MeV)	Absolute γ-ray intensity(I) (13.2 MeV)	Absolute γ-ray intensity(I) (14.8 MeV)	Transition	$E_\gamma = E_f \rightarrow E_i$ (keV)
538.5	492.3±25.3	564.8±28.6	372.6±19.4	196.0±10.6	$4^+ \rightarrow 4^+$	601.8→63.3
570.1	938.4±47.6	1104.9±55.6	704.9±36.1	384.1±19.9	$3^+ \rightarrow 4^+$	633.5→63.3
601.8	1703.6±86.2	1845.5±93.7	1152.9±66.4	662.9±36.7	$4^+ \rightarrow 5^+$	601.8→0
873.3	1070.1±54.7	1227.6±62.0	795±41.1	409.99±26.4	$3^+ \rightarrow 4^+$	936.6→63.3
906.2	479.3±25.1	575.1±29.4	364.5±23.5	188.7±13.2	$2^+ \rightarrow 3^+$	1539.8→633.3

Table 4.1: *The level energies E_γ, absolute intensities (I) and spin assignments at four beam energies for the ^{208}Bi nuclei.*

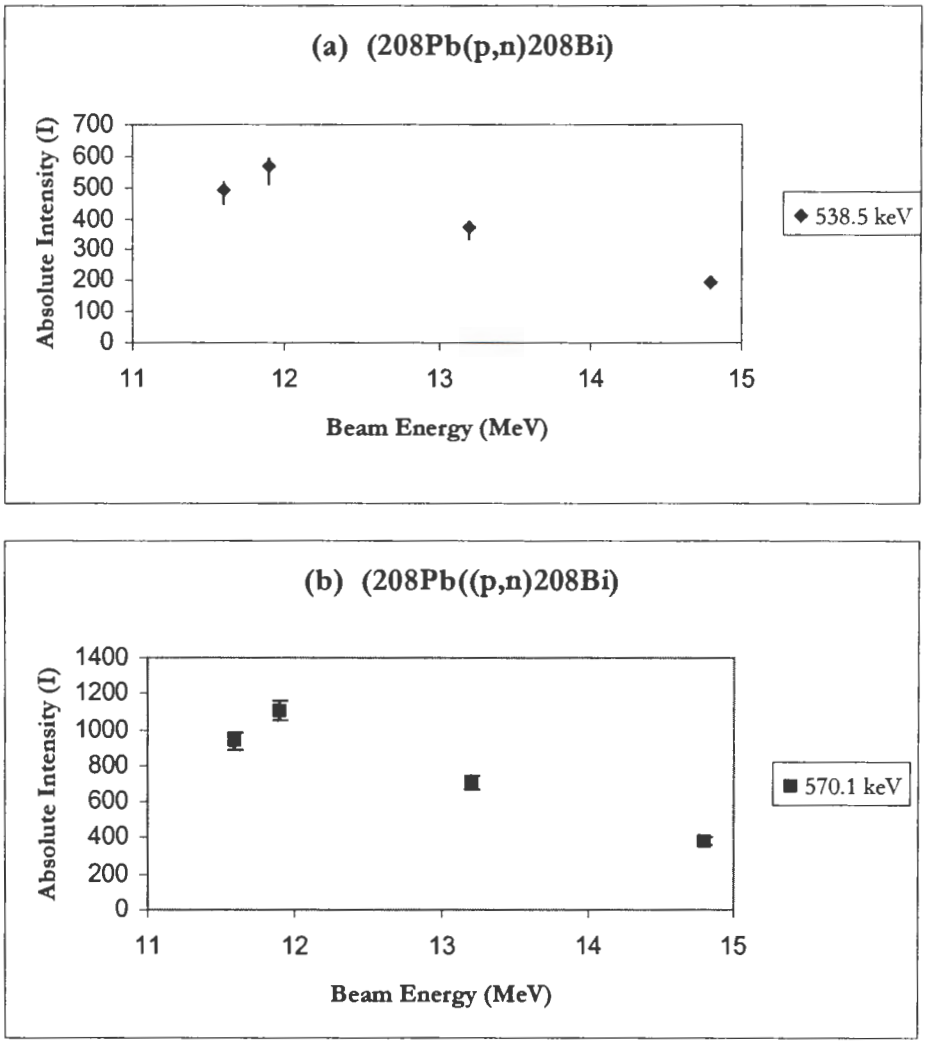

Figure 4.7 (a-b): *Excitation functions for the reaction product, ^{208}Bi, for (a) 538.5 keV and (b) 570.1 keV transitions.*

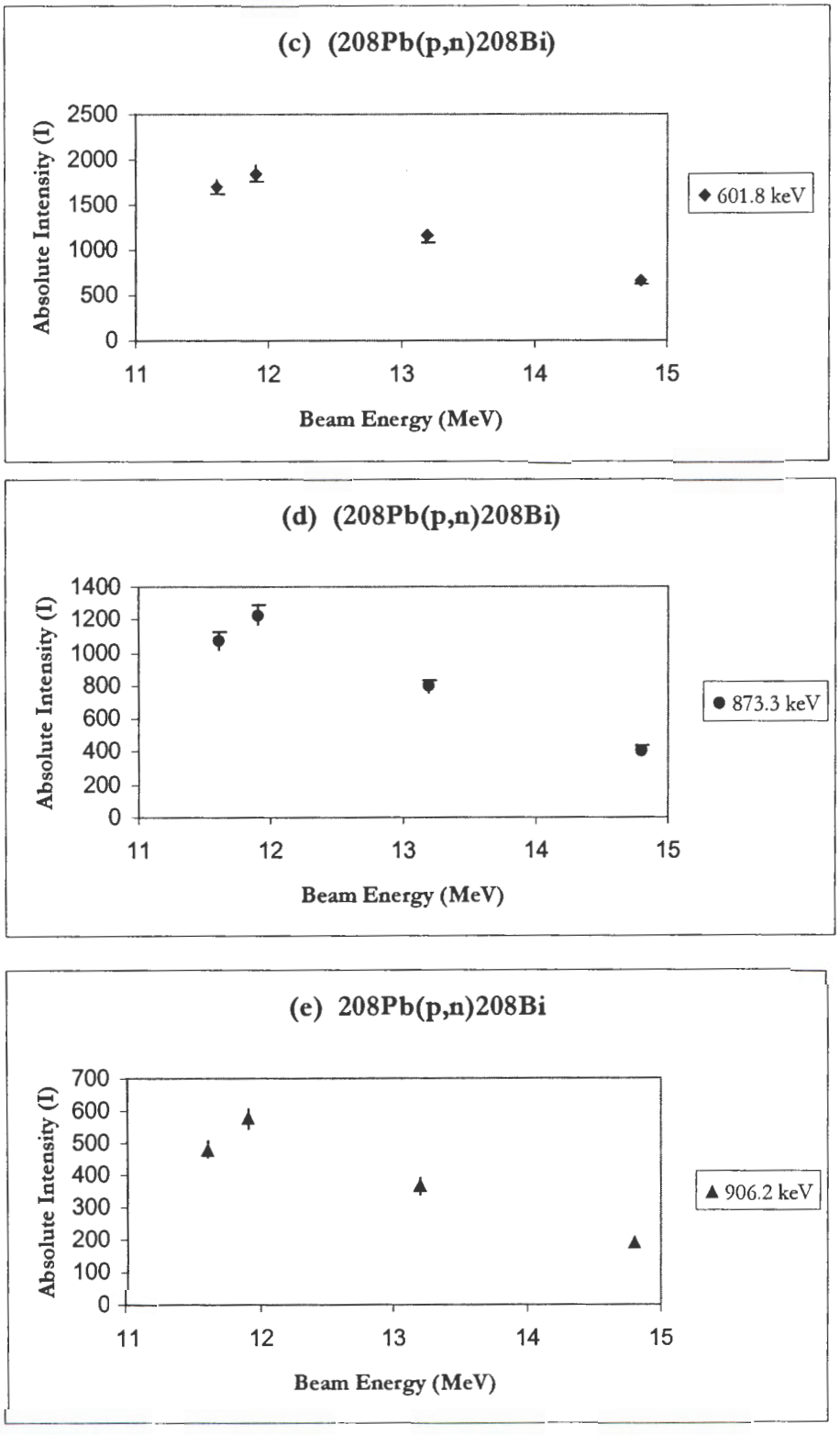

Figure 4.7 (continued) (c-e): *Excitation functions for the reaction product, ^{208}Bi, for (c) 601.8 keV, (d) 873.3 keV and (e) 906.2 keV transitions.*

E_γ (keV)	Relative γ-ray intensity(%) (11.6 MeV)	Relative γ-ray intensity(%) (11.9 MeV)	Relative γ-ray intensity(%) (13.2 MeV)	Relative γ-ray intensity(%) (14.8 MeV)	Transition	$E_\gamma = E_f \rightarrow E_i$ (keV)
538.5	28.9±2.1	30.6±2.2	32.3±2.5	29.6±8.2	$4^+ \rightarrow 4^+$	601.8→63.3
570.1	55.1±4.0	59.9±4.1	61.1±4.7	57.9±4.4	$3^+ \rightarrow 4^+$	633.5→63.3
601.8	100.0±5.1	100.0±5.1	100.0±5.8	100.0±5.5	$4^+ \rightarrow 5^+$	601.8→0
873.3	62.8±4.5	66.5±4.7	68.9±5.3	61.8±5.3	$3^+ \rightarrow 4^+$	936.6→63.3
906.2	28.14±2.1	31.2±2.2	31.6±2.0	28.5±2.5	$2^+ \rightarrow 3^+$	1539.8→633.3

Table 4.2: *Excitation functions for the ^{208}Bi residual nuclei normalised to the 601.8 keV transition.*

4.3 ^{207}Bi γ-γ coincidences

From the spectra obtained, the four most intense ^{207}Bi peaks were chosen for analysis for the 14.8 MeV beam energy as discussed in section 3.6 above. Since ^{207}Bi start to populate more at 13.2 MeV energy, the γ-γ coincidences for the 11.6 MeV, 11.9 MeV and 13.2 MeV beam energies are not considered due to insufficient counts. The peaks considered for the γ-γ coincidence are the 629.8 keV, 669.6 keV and 742.6 keV and 1211.5 keV ^{207}Bi transitions. From the γ-ray coincidence spectra, γ-ray transitions due to the ^{208}Pb(p,2n)^{207}Bi reaction are observed. The resulting γ-ray coincidence spectra representing single gates set on 629.8 keV, 669.6 keV, 742.6 keV and 1211.5 keV transitions are plotted in figures 4.9 – 4.12. Partial decay level schemes [Sch71] for the transitions discussed in this section (section 4.3, figures 4.9 – 4.12) are given in figures 4.8 (A) and (B).

The $(5/2)^-$ state at 1372 keV level decays to the $(7/2)^-$ state at 742.6 keV. When a gate is set on the 629.8 keV transition, the coincidence relationship with the 742.6 keV transition can be clearly seen in figure 4.9.

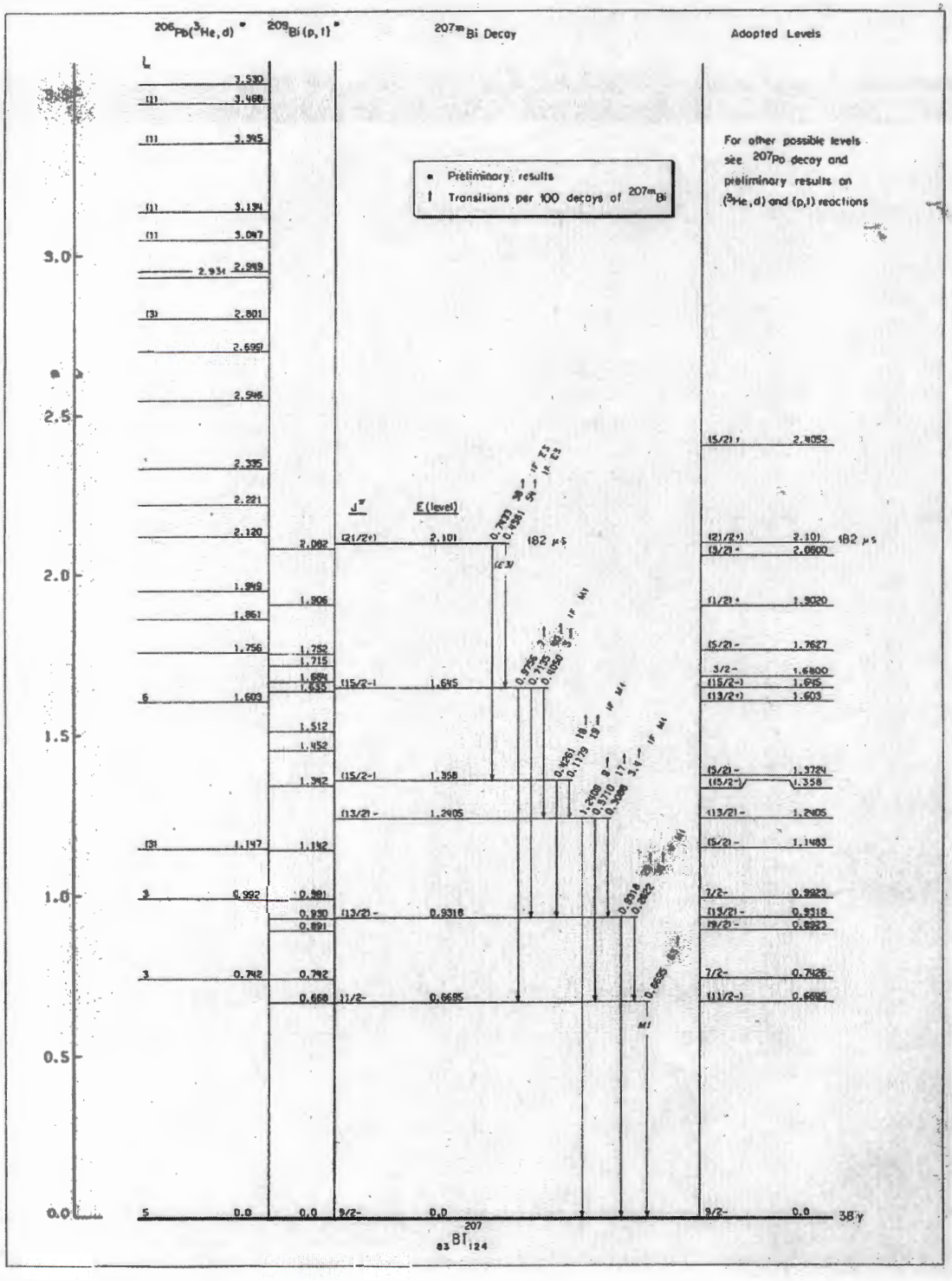

Figure 4.8 (A): *Partial level decay scheme of ^{207}Bi from the transitions depicted in figures 4.9 – 4.12[Sch71].*

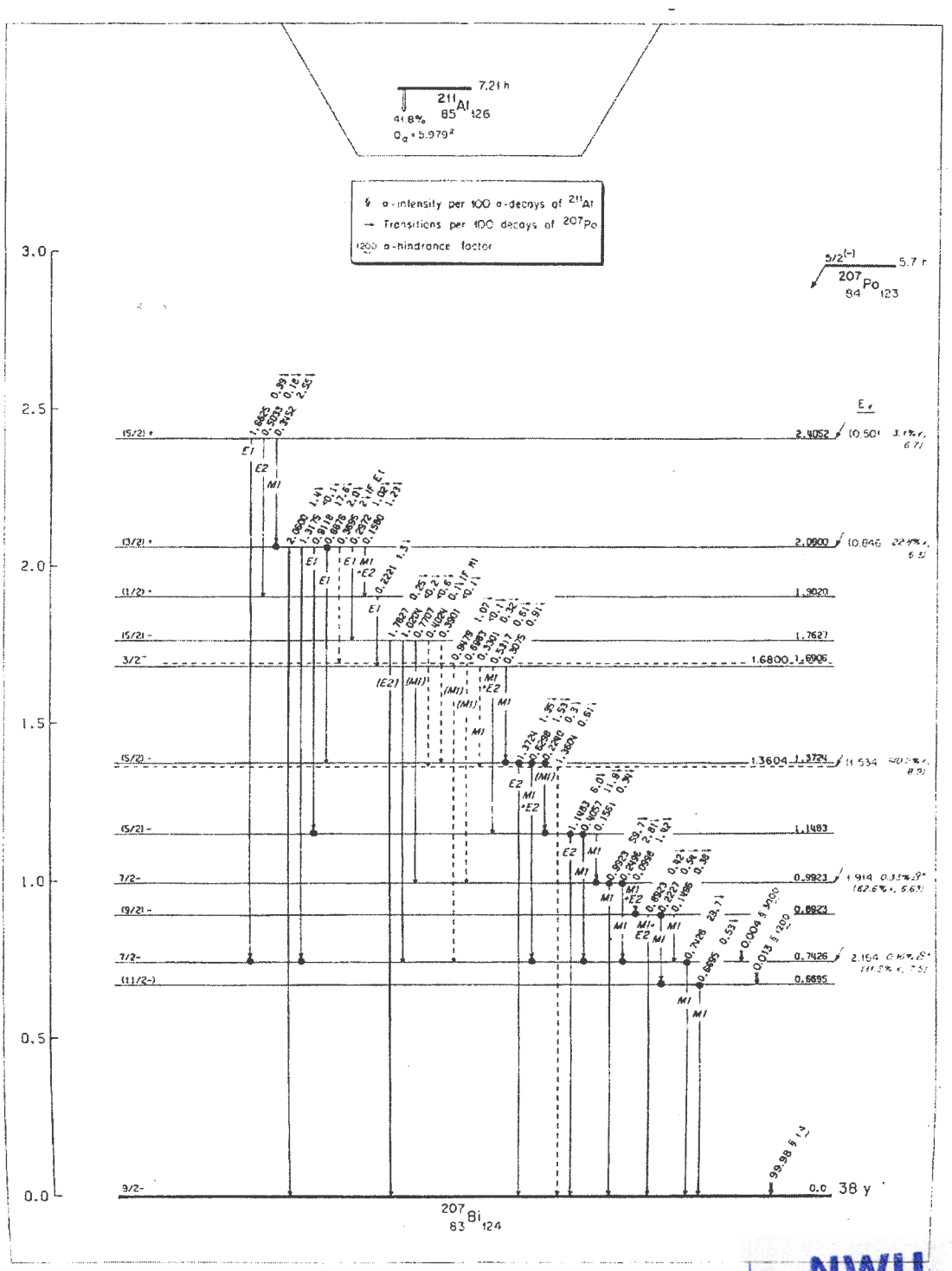

Figure 4.8 (B): *Partial level decay scheme of ^{207}Bi from the transitions depicted in figures 4.9 – 4.12 [Sch71].*

Gating on the 669.6 keV transition results in the spectra shown in figure 4.10 where coincidence relationship with the 571.0 keV transition is clearly seen. The $(11/2)^-$ state at 669.5 keV level makes a $(9/2)^-$ ground state transition as seen in figure 4.8 (A).

There is a strong transition to the $(9/2)^-$ from the 742.6 keV level. When a gate is placed on the 742.6 keV transition, the resulting spectrum shown in figure 4.11 suggest coincidence relationships with the 405.8 keV and 629.8 keV transitions.

Gating on the 1211.5 keV transition results in the spectra shown in figure 4.12 where coincidence relationship with the 571.0 keV transition is clearly seen.

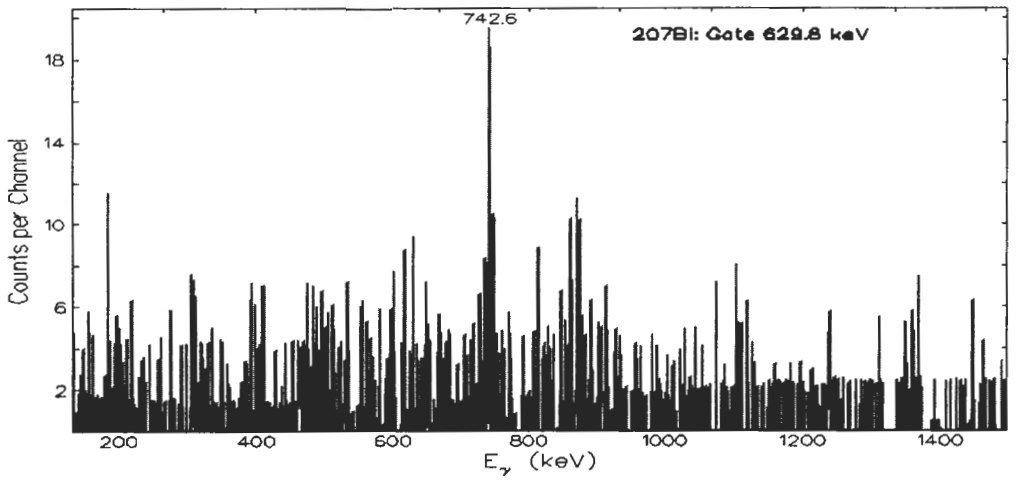

Figure 4.9: *Coincidence γ-ray spectrum gated on the 629.8 keV transition in ^{207}Bi, which shows a coincidence relationship with the 742.6 keV transition.*

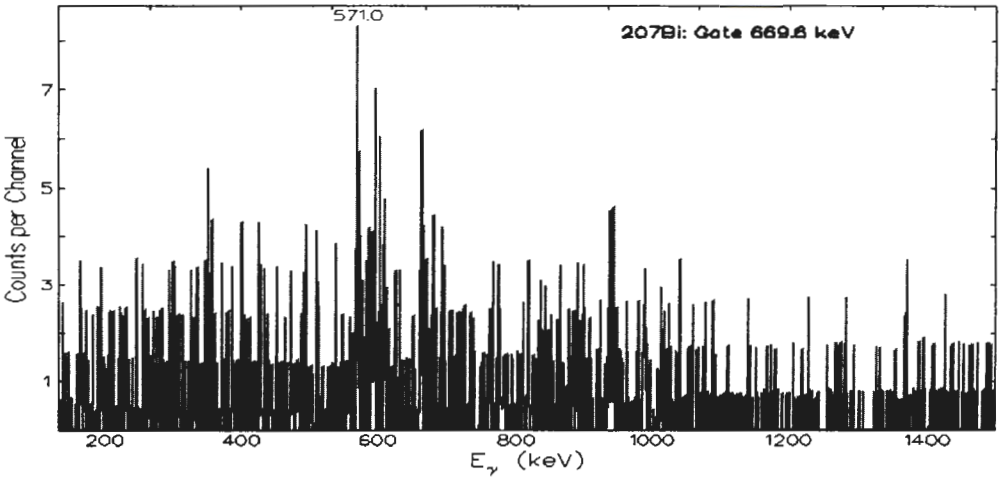

Figure 4.10: *Coincidence γ-ray spectrum gated on the 669.6 keV transition in ^{207}Bi, which shows a coincidence relationship with the 571.0 keV transition.*

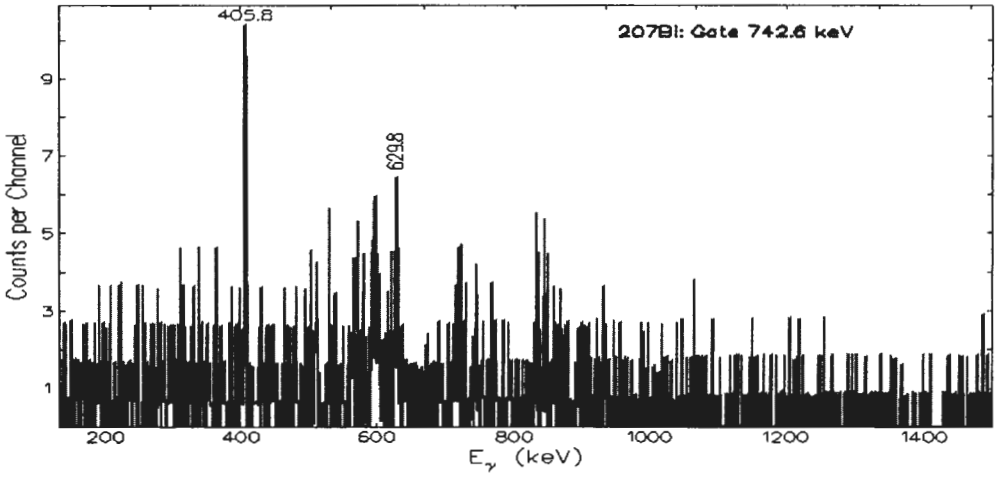

Figure 4.11: *Coincidence γ-ray spectrum gated on the 742.6 keV ^{207}Bi γ-ray transition. The 742.6 keV gate exhibits coincidence relationships with the 405.8 keV and 629.8 keV transitions.*

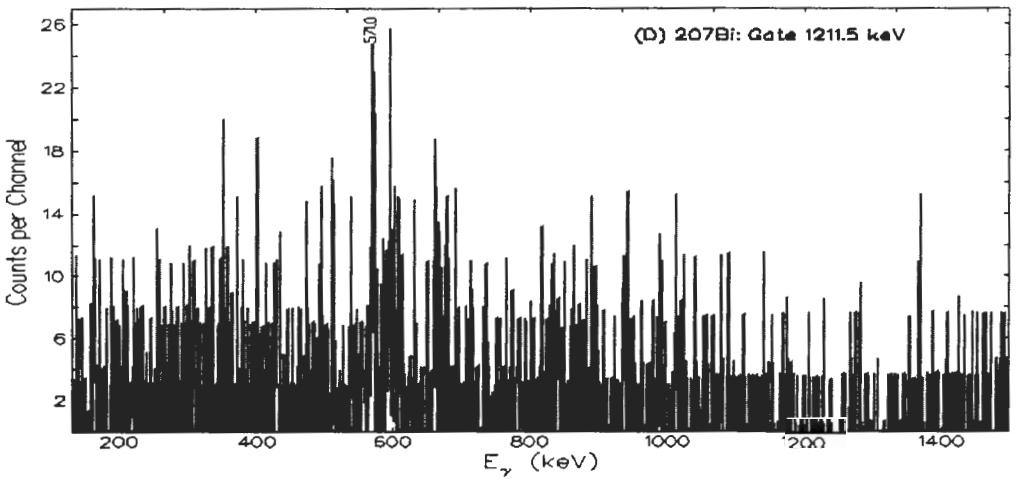

Figure 4.12: *Coincidence γ-ray spectrum gated on the 1211.5 keV ^{207}Bi γ-ray transition. The 1211.5 keV gate exhibit a coincidence relationship with the 571.0 keV transition.*

4.4 Transition Intensities for ^{207}Bi

The relative (I_γ) and absolute γ-ray intensities (I) for the four transitions at four different beam energies were determined from the un-gated γ-ray coincidence spectra and employing equations 3.5 and 3.6 (Appendix 2A). The relative gamma intensities were determined when the peaks were corrected for the detector relative efficiency (assuming 5% uncertainty). The results are listed in table 4.3. The absolute intensity (I) is plotted against the beam energy for each γ-ray transition as shown figures 4.13 (a-d). The relative intensities were normalised to the most intense peak, the 742.6 keV transition, and are listed in table 4.4 (see appendix 2B).

E_γ (keV)	Absolute γ-ray intensity (I) (11.6 MeV)	Absolute γ-ray intensity (I) (11.9 MeV)	Absolute γ-ray intensity (I) (13.2 MeV)	Absolute γ-ray intensity (I) (14.8 MeV)	Transition	$E_\gamma = E_f \rightarrow E_i$ (keV)
629.8	22.2±10.2	28.6±5.3	62.7±8.4	91.1±6.7	$5/2^- \rightarrow 7/2^-$	1372.4→742.6
669.6	12.9±1.6	31.3±0.9	187.6±2.0	762.3±15.5	$11/2 \rightarrow 9/2^-$	669.6→0
742.6	47.4±2.4	86.0±1.8	350.0±7.1	857.3±17.5	$7/2^- \rightarrow 9/2^-$	742.6→0
1211.5	71.2±3.1	73.9±1.6	86.1±1.8	206.7±4.7	$9/2^- \rightarrow 9/2^-$	1211.5→0

Table 4.3: *The level energies E_γ, absolute intensities (I) and spin assignments at four beam energies for the ^{207}Bi nuclei.*

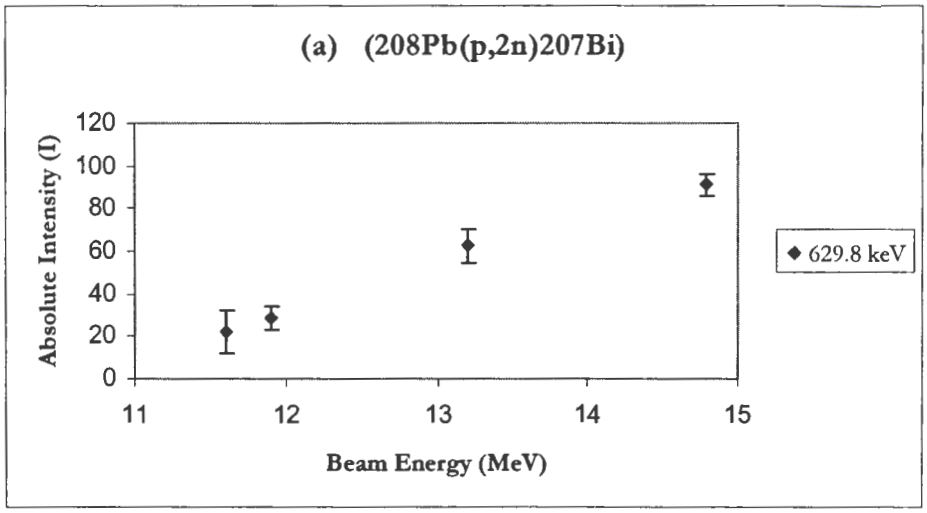

Figure 4.13 (a): *Excitation function for the reaction product, ^{207}Bi, for the 629.8 keV transition.*

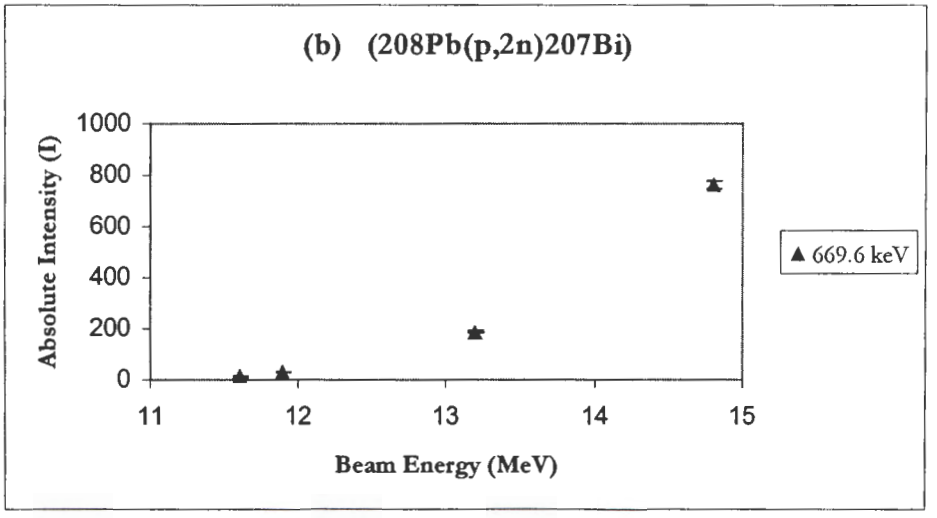

Figure 4.13 (b): *Excitation function for the reaction product, ^{207}Bi, for the 669.6 keV transition.*

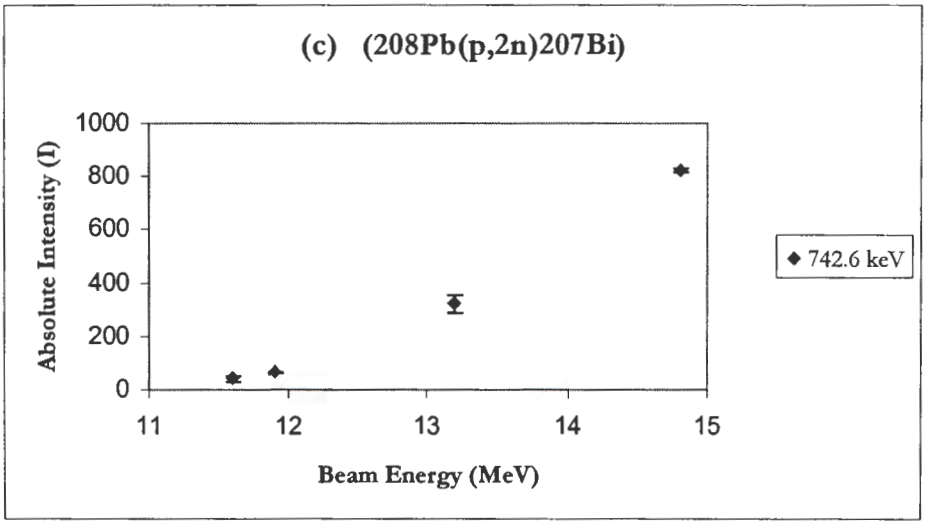

Figure 4.13 (c): *Excitation function for the reaction product, ^{207}Bi, for the 742.6 keV*

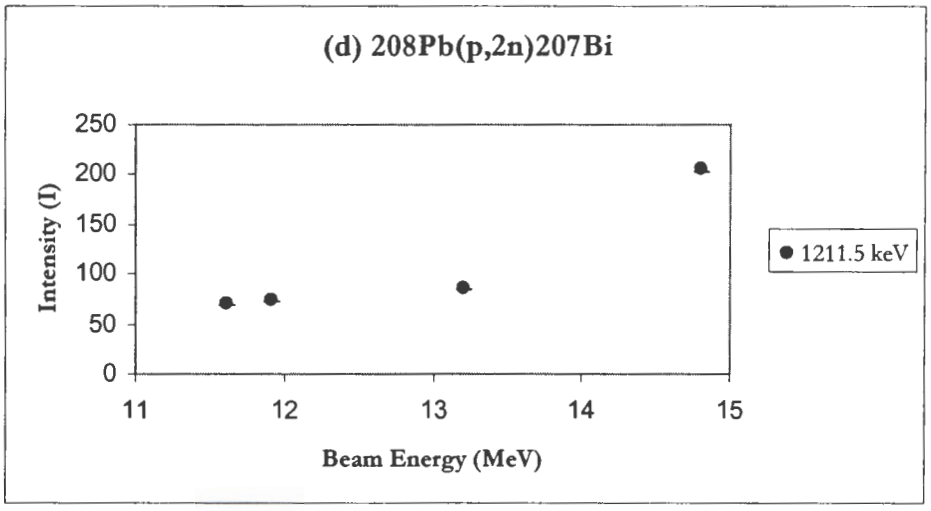

Figure 4.13 (d): *Excitation function for the reaction product, ^{207}Bi, for the 1211.5 keV transitions.*

E_γ (keV)	Relative γ-ray intensity (%) (11.6 MeV)	Relative γ-ray intensity (%) (11.9 MeV)	Relative γ-ray intensity (%) (13.2 MeV)	Relative γ-ray intensity (%) (14.8 MeV)	Transition	$E_\gamma = E_f \rightarrow E_i$ (keV)
629.8	46.8±21.8	28.6±5.1	62.7±7.8	91.1±4.9	$5/2^- \rightarrow 7/2^-$	1372.4→742.6
669.6	27.2±3.6	36.4±1.3	53.6±1.2	89.0±2.6	$11/2^- \rightarrow 9/2^-$	669.6 → 0
742.6	100.0±5.1	100.0±2.0	100.0±2.1	100.0±2.0	$7/2^- \rightarrow 9/2^-$	742.6 → 0
1211.5	150.2±10.0	85.6±2.6	24.6±0.7	24.1±0.6	$9/2^- \rightarrow 9/2^-$	1211.5 → 0

Table 4.4: *Excitation functions for the ^{207}Bi residual nuclei normalised to the 742.6 keV transition.*

4.5 Discussion

The excitation functions observed in sections 4.2 and 4.4 showed the dependence of the ^{207,208}Bi populations on the proton energy. The results presented in table 4.1 and figures 4.7(a-e), show marked increase in the intensity of all the ^{208}Bi γ-ray transitions when the beam energy is increased from E_p = 11.6 MeV to 11.9 MeV. At the beam energy of 11.9 MeV, we have the maximum intensity values for the ^{208}Bi formed due the reaction ^{208}Pb(p,n)^{208}Bi. An increase in beam energy to 13.2 MeV and 14.8 MeV is accompanied by a gradual decrease in the intensity of the ^{208}Bi that is being formed. The increase and subsequent gradual decrease in intensity with increasing beam energy shows a gaussian-like shape as predicted in figure 1.4 (section 1). Lower beam energies, namely, 11.6 MeV and 11.9 MeV, favour the ^{208}Pb(p,n)^{208}Bi reaction. As the beam energy is increased, more energy is given to the compound nucleus, thus increasing the likelihood of more neutrons 'evaporating' from the compound nucleus. This is indicated by the decrease in the intensities, and hence, the statistical distribution of the ^{208}Bi when the beam energy is 13.2 MeV. Continuous increase in the beam energy to 14.8 MeV decreases the population of the ^{208}Bi formed as more neutrons will have enough energy to evaporate from the compound nucleus. This will favour the (p,2n) reaction most.

Table 4.3 and figures 4.13 (a-d) show the population of the ^{207}Bi with increasing beam energy. At low proton energies, namely 11.6 MeV and 11.9 MeV, there is virtually very little or no ^{207}Bi formed. At energies above 11.9 MeV, the ^{208}Pb(p,2n)^{207}Bi reaction becomes energetically possible, prompting more of the ^{207}Bi start to populating. This is because an increase in beam energy increases the energy of the compound nucleus, thus increasing the probability of two neutrons evaporating from the nucleus. This is indicated in figure 4.14 and figure 4.15.

Therefore the (p,2n) threshold determined from the excitation functions above is around 12 MeV. Protons of energies below 12 MeV (11.6 MeV and 11.9 MeV) will predominantly induce a (p,n) reaction. Above the 12 MeV threshold, peaks associated with the (p,2n) reaction products, ^{207}Bi, start to be more prominent in the spectrum. This is indicated in figures 4.14 and 4.15, where ^{207}Bi starts to dominate the population of the reaction products in the spectrum when the beam energy is greater than 12 MeV.

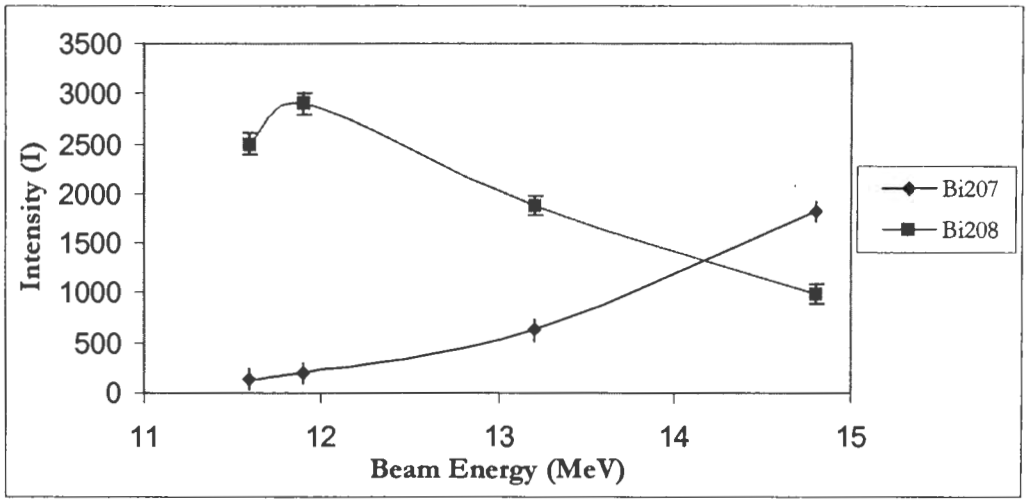

Figure 4.14: *Excitation functions for the sum of the 4^+ ^{208}Bi and the $(9/2)^-$ ^{207}Bi ground state transitions as a function of beam energy. At beam energies below 12 MeV, more of the ^{208}Bi is formed, but as the beam energy increases, an additional neutron starts to evaporate from the compound nucleus, thus prompting the formation of the ^{207}Bi. This is marked by a decrease in the intensity of the ^{208}Bi at higher energies, accompanied by a corresponding increase in ^{207}Bi intensity.*

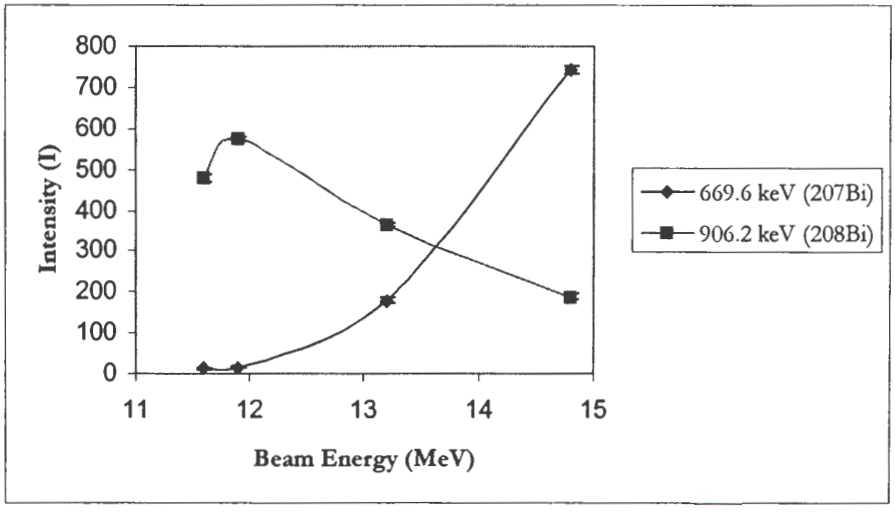

Figure 4.15: *Excitation functions for the ^{208}Bi (906.2 keV) and ^{207}Bi (669.6 keV).*

Chapter 5

Summary and conclusion

This project is based on the study of the excitation functions in ^{207}Bi and ^{208}Bi associated with the bombardment of a thin ^{208}Pb target with a proton beam at energies of 11.6 MeV, 11.9 MeV, 13.2 MeV and 14.8 MeV. The techniques of γ-ray spectroscopy using the AFRODITE array have been employed to investigate the population of the residual ^{207,208}Bi nuclei formed from the reaction ^{208}Pb(p,xn)^{207,208}Bi (x = 1 and 2). The data analysis consists of the identification of γ-ray transitions associated with the de-excitation of the residual ^{208}Bi and ^{207}Bi nuclei, γ-γ coincidence relationships and the γ-intensity measurements.

The angular momentum transfer characterizing the reaction between a small incident proton and a large target nucleus, the ^{208}Pb, is very low, randomly distributed and depends on the impact parameter. Because of the small amount of the angular momentum transferred, a 14 MeV proton incident on a fairly large nucleus, results in angular momentum $l_{max} \approx 5$. This is due to the random collision between the nucleons inside the compound nucleus as the excitation energy is increased. This will enhance evaporation of the neutrons rather than the protons because the Coulomb barrier to be overcomed during the evaporation process further restricts the protons. Therefore more energy is needed to overcome the Coulomb barrier in protons so that they can be evaporated from the compound nucleus. From the results presented, it can be deduced that the experiment was a success, although there were some limitations that need to be pointed out. Such limitations resulted in insufficient data being acquired, especially with reference to the ^{207}Bi nuclei formed.

- We obtained the excitation functions of the ^{208}Bi, showing the variation of the intensity of the gamma radiation with the proton energy. Relative γ-ray intensities of the ^{208}Bi were consistent with beam energy variation, the maximum average error difference in the relative intensities being ± 5%. This is relatively low, thus providing

improved results as compared to previous results, where in some instances, errors were up to 8% [Bon68].

- At low beam energies, particularly 11.6 MeV and 11.9 MeV, ^{207}Bi was weakly populated, particularly the 629.8 keV transition, which had the highest percentage errors in the relative intensity (as shown in table 4.4 and figure 4.13(a)). This is due to the decay of the compound nucleus proceeding primarily through single neutron emission at the lower beam energies.

- As predicted by the compound nucleus model, there is an increase in the intensity of the ^{208}Bi, followed by a decrease as the beam energy is increased. This increase in beam energy is accompanied by the evaporation of an additional neutron, thus resulting in the decrease in the ^{208}Bi population and subsequent increase in the ^{207}Bi population.

There is a need for improvement on the experiment, especially for data relating to the ^{207}Bi formed. In future work, it is important that we have maximum amount of the proton beam hitting the target in order to obtain maximum data rates. The 2n-excitation functions will be complete if we can study higher beam energies, so that the dependence of the ^{207}Bi production on the beam energy can be delineated so that the beam energy that corresponds to the maximum intensity values of ^{207}Bi, can be found. Overall, the measurements were successful.

Appendix 1A

Determination of the absolute γ-ray transition intensities (I) for the ^{208}Bi residual nuclei from the un-gated spectra at four proton energies.

From equations 3.5 and 3.6 as well as figure 3.2 (to determine the efficiency, ϵ), the 'relative' amount of the ^{208}Bi formed as a function of proton energy, without considering the integrated beam, I_γ, is given by

Relative Intensity = Number of counts / efficiency

$$I_\gamma = S/(\epsilon + \Delta\epsilon)$$

Where $\Delta\epsilon = 5\%\ \epsilon$.

The 'absolute' amount of the products at different proton energies (or Intensity) I, is given by:

Intensity = relative intensity / Integrated beam

$$I = S/\epsilon I_E = I_\gamma / I_E$$

The method of determination of the absolute γ-ray intensities is indicated in CASE 1, E_γ = 538.6keV. The same approach is applied to the rest of the other cases.

CASE 1: Beam Energy (E_p) = 11.6 MeV
Integrated Beam ($I_E = I_{11.6\,MeV}$) = 1.78 mAs

1. **E_γ = 538.6 keV (ϵ = 36.2% and $\Delta\epsilon$ = 1.8)**

$$I = \left[\frac{31547 \pm 361}{36.2 \pm 1.8}\right] \times \frac{1}{1.78} = \frac{876.31}{1.78} \pm \frac{876.31}{1.78}\left[\frac{361^2}{31547^2} + \frac{1.8^2}{361^2}\right]^{\frac{1}{2}}$$

$$= 492.3 \pm 25.3$$

2. **E_γ = 570.1 keV (ϵ = 35.1% and $\Delta\epsilon$ = 1.8)**

$$I = \left[\frac{58465 \pm 505}{35.1 \pm 1.8}\right] \times \frac{1}{1.78} = 938.4 \pm 47.6$$

3. **E_γ = 601.8 keV (ϵ = 31.0% and $\Delta\epsilon$ = *1.6*)**

$$I = \left[\frac{94004 \pm 710}{31.0 \pm 1.6}\right] \times \frac{1}{1.78} = 1703.6 \pm 86.2$$

4. **E_γ = 873.3 keV (ϵ = 25.2% and $\Delta\epsilon$ =*1.3*)**

$$I = \left[\frac{47618 \pm 495}{25.2 \pm 1.3}\right] \times \frac{1}{1.78} = 1070.1 \pm 54.7$$

5. **E_γ = 906.2 keV (ϵ = 25.0% and $\Delta\epsilon$ =*1.3*)**

$$I = \left[\frac{21328 \pm 333}{25.0 \pm 1.3}\right] \times \frac{1}{1.78} = 497.3 \pm 25.1$$

CASE 2: Beam Energy (E_p) = 11.9 MeV
Integrated Beam ($I_E = I_{11.9\,MeV}$) = 2.96 mAs

1. **E_γ = 538.6 keV (ϵ = 36.2%)**

$$I = \left[\frac{60187 \pm 500}{36.2 \pm 1.8}\right] \times \frac{1}{2.96} = 564.8 \pm 28.6$$

2. **E_γ = 570.1 keV (ϵ = 35.1%)**

$$I = \left[\frac{114463 \pm 662}{35.1 \pm 1.8}\right] \times \frac{1}{2.96} = 1104.9 \pm 55.6$$

3. **E_γ = 601.8 keV (ϵ = 31.0%)**

$$I = \left[\frac{169342 \pm 1474}{31.0 \pm 1.6}\right] \times \frac{1}{2.96} = 1845.5 \pm 54.7$$

4. **E_γ = 873.3 keV (ϵ = 25.2%)**

$$I = \left[\frac{90845 \pm 626}{25.2 \pm 1.3}\right] \times \frac{1}{2.96} = 1227.6 \pm 62.0$$

5. **E_γ = 906.2 keV (ϵ = 25.0%)**

$$I = \left[\frac{42553 \pm 434}{25.0 \pm 1.3}\right] \times \frac{1}{2.96} = 576.0 \pm 29.4$$

CASE 3: Beam Energy (E_p) = 13.2 MeV
Integrated Beam ($I_E = I_{13.2\,MeV}$) = 2.61 mAs

1. **E_γ = 538.6 keV (ϵ = 36.2%)**

$$I = \left[\frac{35009 \pm 521}{36.2 \pm 1.8}\right] \times \frac{1}{2.61} = 372.6 \pm 19.4$$

2. **E_γ = 570.1 keV (ϵ = 35.1%)**

$$I = \left[\frac{64395 \pm 727}{35.1 \pm 1.8}\right] \times \frac{1}{2.61} = 704.9 \pm 36.1$$

3. **E_γ = 601.8 keV (ϵ = 31.0%)**

$$I = \left[\frac{93280 \pm 2661}{31.0 \pm 1.6}\right] \times \frac{1}{2.61} = 1152.9 \pm 66.4$$

4. **E_γ = 873.3 keV (ϵ = 25.2%)**

$$I = \left[\frac{51926 \pm 673}{25.2 \pm 1.3}\right] \times \frac{1}{2.61} = 795.0 \pm 41.1$$

5. **E_γ = 906.2 keV (ϵ = 25.0%)**

$$I = \left[\frac{22850 \pm 399}{25.0 \pm 1.6}\right] \times \frac{1}{2.61} = 364.5 \pm 23.5$$

CASE 4: Beam Energy (E_p) = 14.8 MeV
Integrated Beam ($I_E = I_{14.8\,MeV}$) = 2.49 mAs

1. **E_γ = 538.6 keV (ϵ = 36.2%)**

$$I = \left[\frac{17568 \pm 351}{36.2 \pm 1.8}\right] \times \frac{1}{2.49} = 196.0 \pm 10.6$$

2. **E_γ = 570.1 keV (ϵ = 35.1%)**

$$I = \left[\frac{33471 \pm 441}{35.1 \pm 1.8}\right] \times \frac{1}{2.49} = 384.1 \pm 19.9$$

3. **E_γ = 601.8 keV (ϵ = 31.0%)**

$$I = \left[\frac{51169 \pm 1208}{31.0 \pm 1.6}\right] \times \frac{1}{2.49} = 662.9 \pm 36.7$$

4. **E_γ = 873.3 keV (ϵ = 25.2%)**

$$I = \left[\frac{2552 \pm 451}{25.2 \pm 1.3}\right] \times \frac{1}{2.49} = 410.0 \pm 26.4$$

5. **E_γ = 906.2 keV (ϵ = 25.0%)**

$$I = \left[\frac{11745 \pm 383}{25.0 \pm 1.6}\right] \times \frac{1}{2.49} = 188.7 \pm 13.2$$

Appendix 1B

Determination of the relative γ-ray transition intensities (%I_γ) for the ^{208}Bi residual nuclei normalized to the 602keV transition.

The calculation method of the relative γ-ray intensities is indicated in CASE 1, E_γ = 538.6keV. The same approach is applied to the rest of the other cases.

CASE 1: Beam Energy (E_p) = 11.6 MeV

1. E_γ = **538.6 keV**

$$I(\%) = \left[\frac{492.3 \pm 25.3}{1703.6 \pm 86.2}\right] \times 100 = 28.9 \pm 2.1$$

2. E_γ = **570.1 keV**

$$I(\%) = \left[\frac{938.4 \pm 47.6}{1703.6 \pm 86.15}\right] \times 100 = 55.1 \pm 4.0$$

3. E_γ = **601.8 keV**

$$I(\%) = 100.0 \pm (\text{fractional error}) = 100.0 \pm \left[\frac{86.2}{1703.6}\right] \text{ x } 100 = 100.0 \pm 5.1$$

4. E_γ = **873.3 keV**

$$I(\%) = \left[\frac{1070.1 \pm 54.6}{1703.6 \pm 86.2}\right] \times 100 = 62.8 \pm 4.5$$

5. E_γ = **906.2 keV**

$$I(\%) = \left[\frac{479.3 \pm 25.1}{1703.6 \pm 86.2}\right] \times 100 = 28.4 \pm 2.1$$

CASE 2: Beam Energy (E_p) = 11.9 MeV

1. E_γ = **538.6 keV**

$$I(\%) = \left[\frac{564.8 \pm 28.6}{1845.5 \pm 93.7}\right] \times 100 = 30.6 \pm 2.2$$

2. E_γ = **570.1 keV**

$$I(\%) = \left[\frac{1104.9 \pm 55.6}{1845.5 \pm 93.7}\right] \times 100 = 59.9 \pm 4.1$$

3. E_γ = **601.8 keV**

$$I(\%) = 100.0 \pm (\text{fractional error}) = 100.0 \pm \left[\frac{93.7}{1845.5}\right] \text{ x } 100 = 100.0 \pm 5.1$$

4. $\mathbf{E_\gamma = 873.3\ keV}$

$$I(\%) = \left[\frac{1227.6 \pm 62.0}{1845.5 \pm 93.7}\right] \times 100 = 66.5 \pm 4.8$$

5. $\mathbf{E_\gamma = 906.2\ keV}$

$$I(\%) = \left[\frac{575.0 \pm 29.4}{1845.5 \pm 93.7}\right] \times 100 = 31.2 \pm 2.3$$

CASE 3: Beam Energy (E_p) = 13.2 MeV

1. $\mathbf{E_\gamma = 538.6\ keV}$

$$I(\%) = \left[\frac{372.6 \pm 19.4}{1152.9 \pm 66.4}\right] \times 100 = 31.2 \pm 2.5$$

2. $\mathbf{E_\gamma = 570.1\ keV}$

$$I(\%) = \left[\frac{704.9 \pm 36.1}{1152.9 \pm 66.4}\right] \times 100 = 61.1 \pm 4.7$$

3. $\mathbf{E_\gamma = 601.8\ keV}$

$$I(\%) = 100.0 \pm (\text{fractional error}) = 100.0 \pm \left[\frac{66.4}{1152.9}\right] \text{ x } 100 = 100 \pm 5.8$$

4. $\mathbf{E_\gamma = 873.3\ keV}$

$$I(\%) = \left[\frac{795.0 \pm 41.1}{1152.9 \pm 66.4}\right] \times 100 = 68.9 \pm 5.3$$

5. $\mathbf{E_\gamma = 906.2\ keV}$

$$I(\%) = \left[\frac{364.5 \pm 23.5}{1152.9 \pm 66.4}\right] \times 100 = 31.6 \pm 2.0$$

CASE 4: Beam Energy (E_p) = 14.8 MeV

1. $\mathbf{E_\gamma = 538.6\ keV}$

$$I(\%) = \left[\frac{196.0 \pm 10.6}{662.9 \pm 36.7}\right] \times 100 = 29.6 \pm 8.2$$

2. $\mathbf{E_\gamma = 570.1\ keV}$

$$I(\%) = \left[\frac{384.1 \pm 19.9}{662.9 \pm 36.7}\right] \times 100 = 57.9 \pm 4.4$$

3. $\mathbf{E_\gamma = 601.8\ keV}$

$$I(\%) = 100.0 \pm (\text{fractional error}) = 100.0 \pm \left[\frac{36.7}{662.9}\right] \text{ x } 100 = 100.0 \pm 5.5$$

4. $\mathbf{E_\gamma = 873.3\ keV}$

$$I(\%) = \left[\frac{410.0 \pm 26.4}{662.9 \pm 36.7}\right] \times 100 = 61.8 \pm 5.3$$

5. E_γ = 906.2 keV

$$I(\%) = \left[\frac{188.7 \pm 13.2}{662.9 \pm 36.7}\right] \times 100 = 28.5 \pm 2.5$$

Appendix 2A

Determination of the absolute γ-ray transition intensities (I) for the ^{207}Bi residual nuclei from the un-gated spectra at four proton energies.

The calculation method is explained in Appendix 1A.

CASE 1: Beam Energy (E_p) = 11.6 MeV
Integrated Beam ($I_E = I_{11.6\,MeV}$) = 1.78 mAs

1. E_γ = 629.8 keV (ϵ = 30.5%)

$$I = \left[\frac{1207 \pm 552}{30.5 \pm 1.5}\right] \times \frac{1}{1.78} = 22.2 \pm 10.2$$

2. E_γ = 669.6 keV (ϵ = 30.0%)

$$I = \left[\frac{689 \pm 146}{30.0 \pm 1.5}\right] \times \frac{1}{1.78} = 12.9 \pm 1.6$$

3. E_γ = 742.6 keV (ϵ = 29.5%)

$$I = \left[\frac{2490 \pm 186}{29.5 \pm 1.5}\right] \times \frac{1}{1.78} = 47.4 \pm 2.4$$

4. E_γ = 12115 keV (ϵ = 20.0%)

$$I = \left[\frac{2534 \pm 146}{20.0 \pm 1.0}\right] \times \frac{1}{1.78} = 71.2 \pm 3.1$$

CASE 2: Beam Energy (E_p) = 11.9 MeV
Integrated Beam ($I_E = I_{11.9\,MeV}$) = 2.96 mAs

1. E_γ = 629.8 keV (ϵ = 30.5%)

$$I = \left[\frac{2581 \pm 462}{30.5 \pm 1.5}\right] \times \frac{1}{2.96} = 28.6 \pm 5.3$$

2. E_γ = 669.6 keV (ϵ = 30.0%)

$$I = \left[\frac{2783 \pm 193}{30.0 \pm 1.5}\right] \times \frac{1}{2.96} = 31.3 \pm 0.9$$

3. E_γ = 742.6 keV (ϵ = 29.5%)

$$I = \left[\frac{7511 \pm 245}{29.5 \pm 1.5}\right] \times \frac{1}{2.96} = 86.0 \pm 1.7$$

4. E_γ = 12115 keV (ϵ = 20%)

$$I = \left[\frac{4372 \pm 185}{20.0 \pm 1.0}\right] \times \frac{1}{2.96} = 73.9 \pm 1.6$$

CASE 3: Beam Energy (E_p) = 13.2 MeV
Integrated Beam ($I_E = I_{13.2\,MeV}$) = 2.61 mAs

1. E_γ = 629.8 keV (ϵ = 30.5%)

$$I = \left[\frac{4990 \pm 621}{30.5 \pm 1.5}\right] \times \frac{1}{2.61} = 62.7 \pm 8.4$$

2. E_γ = 669.6 keV (ϵ = 30.0%)

$$I = \left[\frac{14687 \pm 332}{30.0 \pm 1.5}\right] \times \frac{1}{2.61} = 187.6 \pm 2$$

3. E_γ = 742.6 keV (ϵ = 29.5%)

$$I = \left[\frac{26946 \pm 451}{29.5 \pm 1.5}\right] \times \frac{1}{2.61} = 350.0 \pm 7.1$$

4. E_γ = 12115 keV (ϵ = 20.0%)

$$I = \left[\frac{4496 \pm 204}{20.0 \pm 1.0}\right] \times \frac{1}{2.61} = 86.1 \pm 1.8$$

CASE 4: Beam Energy (E_p) = 14.8 MeV
Integrated Beam ($I_E = I_{14.8\,MeV}$) = 2.49 mAs

1. E_γ = 629.8 keV (ϵ = 30.5%)

$$I = \left[\frac{6916 \pm 371}{30.5 \pm 1.5}\right] \times \frac{1}{2.49} = 91.1 \pm 6.7$$

2. E_γ = 669.6 keV (ϵ = 30.0%)

$$I = \left[\frac{56945 \pm 480}{30.0 \pm 1.5}\right] \times \frac{1}{2.49} = 762.3 \pm 15.5$$

3. E_γ = 742.6 keV (ϵ = 29.5%)

$$I = \left[\frac{62970 \pm 522}{29.5 \pm 1.5}\right] \times \frac{1}{2.49} = 857.3 \pm 17.5$$

4. E_γ = 12115 keV (ϵ = 20.0%)

$$I = \left[\frac{10293 \pm 268}{20.0 \pm 1.0}\right] \times \frac{1}{2.49} = 0.2 \pm 4.7$$

Appendix 2B

Determination of the relative γ-ray transition intensities (%I_γ) for the ^{207}Bi residual nuclei normalized to the 742.6 keV transition.

The calculation method of the relative γ-ray intensities is indicated in CASE 1, E_γ = 538.6keV. The same approach is applied to the rest of the other cases.

CASE 1: Beam Energy (E_p) = 11.6 MeV

1. E_γ = 629.8 keV

$$\left[\frac{22.2\pm10.3}{47.4\pm2.4}\right]\times100 = 46.8\pm21.8$$

2. E_γ = 669.6 keV

$$\left[\frac{12.9\pm1.6}{47.4\pm2.4}\right]\times100 = 27.2\pm3.6$$

3. E_γ = 742.6 keV

$$I(\%) = 100.0 \pm (\text{fractional error}) = 100.0 \pm \left[\frac{2.4}{47.4}\right] = 100.0 \pm 5.1$$

4. E_γ = 1211.5 keV

$$\left[\frac{71.2\pm3.1}{47.4\pm2.4}\right]\times100 = 150.1\pm10.0$$

CASE 2: Beam Energy (E_p) = 11.9 MeV

1. E_γ = 629.8 keV

$$\left[\frac{28.6\pm5.3}{86.0\pm1.7}\right]\times100 = 33.2\pm6.2$$

2. E_γ = 669.6 keV

$$\left[\frac{31.3\pm0.9}{86.0\pm1.7}\right]\times100 = 36.4\pm1.3$$

3. E_γ = 742.6 keV

$$I(\%) = 100.0 \pm (\text{fractional error}) = 100.0 \pm \left[\frac{1.7}{86.0}\right] \text{ x } 100 = 100.0 \pm 2.0$$

4. E_γ = 1211.5 keV

$$\left[\frac{73.9\pm1.6}{86.0\pm1.7}\right]\times100 = 85.6\pm2.6$$

CASE3: Beam Energy (E_p) = 13.2 MeV

1. E_γ = 629.8 keV

$$I(\%) = \left[\frac{62.7\pm8.4}{350.0\pm7.1}\right]\times100 = 17.9\pm2.4$$

2. E_γ = 669.6 keV

$$I(\%) = \left[\frac{187.6\pm2}{350.0\pm7.1}\right]\times100 = 53.6\pm1.2$$

3. E_γ = 742.6 keV

$$I(\%) = 100.0 \pm (\text{fractional error}) = 100.0 \pm \left[\frac{7.1}{345.0}\right] \text{ x } 100 = 100.0 \pm 2.1$$

4. E_γ = 1211.5 keV

$$I(\%) = \left[\frac{86.1\pm1.8}{350.0\pm7.1}\right]\times100 = 24.6\pm0.7$$

CASE4: Beam Energy (E_p) = 14.8 MeV

1. E_γ = 629.8 keV

$$\left[\frac{91.1\pm6.7}{857.3\pm17.5}\right]\times100 = 10.6\pm0.8$$

2. E_γ = 669.6 keV

$$\left[\frac{762.3\pm15.5}{857.3\pm17.5}\right]\times100 = 88.9\pm2.6$$

3. E_γ = 742.6 keV

$$I(\%) = 100.0 \pm (\text{fractional error}) = 100.0 \pm \left[\frac{17.5}{857.3}\right] \text{ x } 100 = 100.0 \pm 2.0$$

4. E_γ = 1211.5 keV

$$\left[\frac{206.7\pm4.7}{857.3\pm17.5}\right]\times100 = 24\pm0.6$$

References

[Bar89] R.A. Bark et al., *Configuration-dependent deformations*, Nuclear Physics. **A501**, 157 (1989).

[Bon68] M. Bonitz et al., *Evidence for j-forbidden Isomeric Transition in* ^{208}Bi, Nuclear Physics. **A115,** 219 (1968).

[Dow00] D. Dowie and S. M. Mullins, *B.Sc (Physics) Vacation Project*, University of Western Cape, unpublished, December (2000).

[Eji89] H. Ejiri and M.J.A. de Voigt, *Gamma-ray and electron Spectroscopy in Nuclear Physics,* Clarendon, Oxford, (1989).

[Eml86] H. Emling et al, Nuclear Instruments and Methods in Physics Research. **A249**, 320 (1986).

[Ers64] J. R. Erskine, Physical Review. **135**, B110 (1964).

[Fags] http://www.fags.org/docs/qp/chap03.html.

[Fir96] R. B. Firestone, *Table of Isotope,* 8th Ed., Vol. 1 and 2, John Wiley and Sons, INC, NY, (1996).

[Gab68] W. Gabsdil, *The Isomers* ^{101m}Tc, ^{103m}Ru, ^{158m}Tb *and* ^{208m}Bi, Nuclear Physics. **A120**, 555 (1968).

[Glo01] M. Gloris et al., *Proton-induced production of residual radio nuclides in lead at Intermediate Energies*, Nuclear Instruments and Methods in Physics Research. **A463**, 593 (2001).

[Goo80] C. D. Goodman, S.M. Austin, S.D. Bloom, J. Rapaport and G.R. Satchler, Plenum Press, New York, (1980).

[Gif96] N. Giffin, http://triumf.ca/safety/rpt/rpt_2/node20.html, (1996).

[Gil98] G. Gilmore and J. D. Hemingway, *Practical Gamma-Ray Spectrometry*, John Wiley & Sons Ltd, Chichester, (1998).

[Hag69] G. R. Hagee et al., *Levels and Transitions in ^{208}Bi*, Phys. Lett. 225 (1969).

[Han63] G. B. Hansen et al., *Population of Rotational States by Proton Induced Reactions*, Nuclear Physics **47**, 529 (1963).

[Hod71] P. E. Hodgson, *Nuclear Reactions and Nuclear Structure*, Claredon Press, Oxford (1971).

[Hod97] P. E. Hodgson et al., *Introductory Nuclear Physics,* Claredon Press, Oxford (1997).

[Joh74] P.D. Johnston et al, *Nuclear Magnetic Moment of ^{207}Bi and Reorientation in the 0.8-sec Isomer of ^{207}Pb*, Phys. Rev. Lett **32**, 784 (1974).

[Jon95] P.M. Jones et al, Nuclear Instruments and Methods in Physics Research. **A362**, 556 (1995).

[Kno79] Glenn F. Knoll, *Radiation Detection and Measurement,* John Wiley and Sons, Inc, New York, (1979).

[Kra88] Krane Kenneth S., *Introductory Nuclear Physics*, Wiley and Sons Co, New York, (1988).

[Kwi01] P. Kwinana, MSc Thesis, University of Western Cape, unpublished, (2001).

[Lil01] J. Lilley, *Nuclear Physics*, John Wiley and Sons Ltd, Chimchester, (2001).

[Lip03] M. Lipoglavsek, Private Communication, (2003).

[Lip04] M. Lipoglavsek et al., to be published (2004).

[Mab03] G. K. Mabala, PhD Thesis, University of Cape Town, unpublished, (2003).

[Men71] J. J. H. Menet et al, *Total-Reaction-Cross-Section Measurements for 30-60MeV Protons and the Imaginary Optical Potential,* Physical Review **C4**, 1114 (1971).

[Mic97] R. Michel at al, *Cross sections for the production of residual nuclides by low- and medium-energy protons from the target elements C, N, O, Mg, Al, Si, Ca, Ti, V, Mn, Fe, Co, Ni, Cu, Sr, Y, Zr, Nb, Ba and Au,* Nuclear Instruments and Methods in Physics Research **B129**, 153 (1997).

[MIDAS] http://npg.dl.ac.uk/MIDAS/.

[Mor63] H. Morinaga and P.C. Gugelot, *Gamma rays following (α, xn) reactions*, Nuclear Physics **46,** 210 (1963).

[Mor01] H. Morinaga and T Yamazaki, *In-Beam Gamma-ray Spectroscopy*, North-Holland Publishing Company, (2001).

[New98] R.T. Newman et al., *Proceedings of Balkan School on Nuclear Physics, September 1-10, 1998 Baltalimani*, Istanbul-TURKEY, Balkan Phys. Lett, 182 (1998).

[nndc] http://www.nndc.bnl.gov/htbin/nudat.cgi.

[Pro70] D. Proetel, M. Dost, E. Grosse, H.J. Korner and P. von Brentano, *The γ-decay of Proton-Particle Neutron-hole States in ^{208}Bi,* Nuclear Physics. **A161**, 565 (1970).

[Rad95] D.C. Radford, Nucl. Instr. And Meth. **A361**, 306 (1995).

[Rad00] D. Radford, *http://radware.phy.ornl.gov*, (2000).

[Reu83] U. Reus and W. Westmeier, *Catalog of Gamma Rays from Radioactive Decay-Part I*, Atomic Data and Nuclear Data Tables, Vol.**29**, No. 1, Academic Press, Inc, New York (1983).

[Rup72] T. Rupnik, *Electron-Capture-to-Positron Ratio in ^{207}Bi Decay*, Phys. Rev. **C6**, 1433 (1972).

[Sak65] M. Sakai, T. Yamazaki and H. Ejiri, *Measurement of conversion electrons from (p,2n) reactions on the vibrational nuclei*, Nuclear Physics **74**, 81 (1965).

[Sch71] M.R. Schmorak and R.L. Auble, Nucl. Data **B5**, 212 (1971).

[Sha88] J.F. Sharpey-Schafer and J. Simpson, Prog. Part. Nucl. Phys. **21,** 293 (1988).

[She03] http://shef.ac.uk/physics/teaching/phy303/phy303-5.html.

[The97] http://theory.uwinnipeg.ca/physics/quant/node4.html.